View metadata, citation and similar papers at core.ac.uk
brought to you by CORE
provided by UNT Digital Library

LM-07K002
April 5, 2007

Raman Spectroscopy of n-Type and p-Type GaSb with Multiple Excitation Wavelengths

JE Maslar, WS Hurst, CA Wang

NOTICE

This report was prepared as an account of work sponsored by the United States Government. Neither the United States, nor the United States Department of Energy, nor any of their employees, nor any of their contractors, subcontractors, or their employees, makes any warranty, express or implied, or assumes any legal liability or responsibility for the accuracy, completeness or usefulness of any information, apparatus, product or process disclosed, or represents that its use would not infringe privately owned rights.

Raman Spectroscopy of n-Type and p-Type GaSb with Multiple Excitation Wavelengths

J. E. Maslar*[1], W. S. Hurst[1], and C. A. Wang[2]

[1]Chemical Science and Technology Laboratory, National Institute of Standards and Technology, 100 Bureau Drive, Stop 8360, Gaithersburg, MD 20899-8360

[2]Lincoln Laboratory, Massachusetts Institute of Technology, 244 Wood Street, Lexington, MA 02420-9108

The interpretation of Raman spectra of GaSb can be complicated by the presence of a so-called surface space charge region (SSCR), resulting in an inhomogeneous near-surface Raman scattering environment. To fully interpret Raman spectra, it is important to have an understanding of the SSCR profile relative to the Raman probe depth. However, a priori determination of even the actual SSCR width is not always possible for GaSb under a wide range of doping levels. The primary objective of this report is to provide a convenient reference to aid in the determination of relative contributions to an observed GaSb Raman spectrum of SSCR scattering and bulk scattering for a range of excitation wavelengths, doping levels, and SSCR widths and types. Hence, Raman spectra of both n-type and p-type doped GaSb epilayers were obtained using 488 nm, 514.5 nm, 647.1 nm, and 752.55 nm excitation radiation. Both n-type and p-type doped GaSb epilayers were selected for investigation because these layers exhibit the two different SSCR types that are typically encountered with as-grown GaSb and related

The Lincoln Laboratory portion of this work was sponsored by the Department of Energy (DOE), under Air Force contact number FA8721-05-C-0002. The opinions, interpretations, conclusions and recommendations are those of the authors and are not necessarily endorsed by the United States Government.

materials. A range of doping levels were examined for each doping type so as to examine the effects of a varying SSCR width on the observed spectra. A secondary objective of this report is to demonstrate the performance of a spectroscopic system based on 752.55 nm excitation that is sensitive to bulk carrier properties in n-type and p-type doped GaSb epilayers over a wide doping range, unlike visible wavelength-based optical systems.

Index Headings: GaSb; Raman spectroscopy; surface space charge region; depletion layer; accumulation layer; n-type doping, p-type doping

*Corresponding author: e-mail: jmaslar@nist.gov

Phone: 301-975-4182

INTRODUCTION

GaSb and related alloy semiconductors, e.g., GaInAsSb and GaInSb, are of interest for mid-infrared sources and detectors and low-power, high-speed electronic devices.[1-3] Characterization of these materials at various stages of device fabrication is critical to fabrication process development and a variety of metrologies have been employed for this purpose,[1-3] including Raman spectroscopy.[1,3] Raman spectroscopy can potentially be used to probe numerous materials properties of semiconductor materials, including crystal quality, alloy composition, and carrier concentration and mobility.[4]

Although Raman spectroscopy is a potentially useful technique for characterizing a variety of GaSb material properties, the interpretation of Raman spectra of GaSb and related materials can be complicated by the inhomogeneous nature of the near-surface Raman scattering environment. Compound semiconductor materials exhibit a so-called surface space-charge

region (SSCR) that develops because of the presence of charge-trapping electronic surface states.[5] Depending on the SSCR width relative to Raman probe depth, the observed Raman signal either will originate almost exclusively from the SSCR or from a combination of the SSCR and the bulk. For radiation with wavelengths shorter than ≈600 nm, the absorption coefficient of radiation in GaSb increases significantly and continues to increase as wavelength decreases.[6] Hence, for scattering excitation wavelengths of ≈532 nm or shorter, observed scattering from GaSb results largely from the SSCR and it is difficult, if not impossible, to probe bulk material properties, particularly for epilayers with moderate to low doping levels (and concomitant large SSCR width). Such a situation can lead to obvious problems for spectral interpretation. For example, nominally undoped GaSb is typically lightly p-type doped due to the presence of residual acceptors[3] and spectra of this material excited with 532 nm or shorter wavelength radiation actually reflects the p-type SSCR spectrum. The primary scattering feature in the p-type SSCR spectrum is broadened and shifted in wavenumber with respect to that of nominally undoped bulk GaSb.[7-9] Despite periodic reports pointing out the necessity of selecting an excitation wavelength with a corresponding probe depth greater than the SSCR width in GaSb,[7-11] numerous articles have appeared in the literature in which the authors attempt to infer information about bulk GaSb properties where the excitation radiation is strongly absorbed in the SSCR, i.e., reports in which Raman spectra are excited with 488 nm or 514.5 nm radiation. To fully interpret Raman spectra, especially spectra excited with blue-green wavelength radiation, it is important to have an understanding of the SSCR profile relative to the Raman probe depth.

The determination a priori of even the actual SSCR width using simple models is not always possible for GaSb. This is in part due to the dependence of the SSCR spatial profile upon bulk carrier type and concentration and surface state density, but it is also due to the specific

material properties of GaSb. For n-type GaSb, significant carrier populations exist in the two lowest conduction band minima, even at room temperature and moderate doping levels.[12,13] Hence, the Hall concentration and mobility obtained from single magnetic field Hall effect measurements performed on n-GaSb provide a weighted average of the concentration and mobility of the two types of electrons.[14,15] Therefore, it is not straight forward to relate single magnetic field Hall effect measurements, one of the most widely applied techniques for semiconductor characterization, to electron concentration or donor doping level, which is critical data for use in the relatively simple SSCR models. This is in contrast to n-type GaAs for which relatively simple SSCR models have been shown to work reasonably well.[16] For p-type GaSb, quantum mechanical treatments are generally necessary to accurately describe the SSCR profile.[17,18] Such methods are often difficult to widely apply in a simple manner. Given the potential impact of SSCR scattering on observed Raman spectra and the difficulty is determining SSCR widths, a better understanding of the dependence of SSCR width on carrier/dopant concentration and the relative magnitude of SSCR width to Raman probe depth would be useful in the interpretation of observed spectra and selection of experimental conditions. However, to the authors' knowledge, no systematic investigation of the effects of varying Raman probe depth and SSCR profile on the resulting Raman spectrum have been reported.

The primary objective of this report is to provide a convenient reference to aid in the determination of relative contributions to an observed GaSb Raman spectrum of SSCR and bulk scattering for a range of excitation wavelengths, doping levels, and SSCR widths and types. Such a reference should facilitate a fuller interpretation of observed Raman spectra as well as the inter-comparison of Raman spectra obtained with different excitation wavelengths. To achieve this objective, Raman spectra of both n-type and p-type doped GaSb epilayers were obtained

using 488 nm, 514.5 nm, 647.1 nm, and 752.55 nm excitation radiation. Both n-type and p-type doped GaSb epilayers were selected for investigation because these layers exhibit the two different SSCR types that are typically encountered with as-grown GaSb and related materials. A range of doping levels were examined for each doping type so as to examine the effects of a varying SSCR width on the observed spectra. For n-type epilayers, the SSCR width was calculated from the experimental spectra. For p-type epilayers, the SSCR width as a function hole concentration was estimated from literature reports. Comparisons of the SSCR width to Raman probe depth were used to aid in the determination of the relative contributions to overall scattering signal of scattering originating in the SSCR and in the bulk. A secondary objective of this report is to demonstrate the performance of a Raman spectroscopic system for the characterization of bulk materials properties of GaSb and related materials. This spectroscopic system is based on the 752.55 nm line from a krypton ion laser and is shown to be sensitive to bulk carrier properties in both n-type and p-type doped GaSb epilayers throughout the range of doping levels investigated here, unlike visible wavelength-based optical systems.

EXPERIMENTAL PROCEDURE

Materials. All GaSb epilayers were grown on semi-insulating GaAs substrates in a vertical flow, rotating-disk organometallic vapor phase epitaxy reactor using triethylgallium and trimethylantimony, as previously described.[19,20] Diethyltellurium (DETe) was used as the n-type dopant and dimethylzinc (DMZn) was used as the p-type dopant. Dopant concentrations were controlled by changing the DETe or DMZn mole fraction in the reactor. All epilayers were intentionally doped except for one layer which was grown without dopant precursor flowing in the chamber. The epilayer grown without dopant precursor flow was unintentionally doped (uid) lightly p-type due to the presence of residual acceptor states, as is generally the case with

nominally undoped GaSb epilayers.[3] The most heavily doped p-type epilayer (10×10^{-6} mole fraction DMZn) was grown on (001) GaAs misoriented 2° toward (100). All other epilayers were grown on (001) GaAs misoriented 6° toward $(1\bar{1}1)$B. The uid-GaSb epilayer was nominally 2.5 μm thick and deposited directly on the GaAs substrate. The n-type epilayers were nominally 2.5 μm thick and were deposited on a 0.4 μm thick uid-GaSb buffer layer that was deposited on the substrate. The most heavily doped p-type epilayer (10×10^{-6} mole fraction DMZn) was nominally 3.0 μm thick and was deposited on a 0.1 μm thick uid-GaSb buffer layer that was deposited on the substrate. All other p-type epilayers were nominally 1.9 μm thick and were deposited directly on the substrate.

Hall Effect Measurements. Hole concentration and mobility were determined using single magnetic field (10 KG) Hall effect measurements based on the van der Pauw method and performed at room temperature. As mentioned, the Hall concentration and mobility obtained from single magnetic field Hall effect measurements performed on n-GaSb provide a weighted average of the concentration and mobility of the two types of electrons. This is also the case for p-type III-V materials due to the presence of light and heavy holes.[21,22] While it is possible to approximately estimate the transport properties of two carrier types (electrons or holes) from the single field Hall effect results using an appropriate transport model,[15,22-24] such an analysis is often not performed. Despite the limitations of single magnetic field Hall effect measurements in determining carrier properties in GaSb, the results of such measurements are still widely reported. Hence, the single magnetic field Hall effect measurement results are reported here to facilitate comparison to the work of other investigators.

Secondary Ion Mass Spectrometry Measurements. The atomic Te dopant concentration was determined for n-GaSb using secondary ion mass spectrometry (SIMS) with a

Cs^+ primary ion beam. Calibration of the absolute Te concentration was based on GaSb standards that were ion implanted with Te. SIMS measurements were performed on nominally identical (but different) epilayers to those used for Raman spectroscopic measurements. Comparisons of SIMS results on epilayers with nominally identical N_D values resulted in variations of ≈±10 %.

Raman Spectroscopic Measurements. All Raman spectroscopic measurements were performed at (nominally) room temperature in a backscattering geometry described by $z(x, y)\bar{z}$, where *x*, *y*, *z*, and $\bar{z}$ denote [100], [010], [001], and [$00\bar{1}$], respectively. Raman spectra were obtained using 488 nm and 514.5 nm excitation from an argon ion laser and 647.1 nm and 752.55 nm excitation from a krypton ion laser. For all measurements, an appropriate holographic laser bandpass filter was used to remove laser plasma lines and the polarization of the incident laser beam was selected with a Glan-Taylor prism polarizer. Laser radiation was focused onto the specimen with a 300 mm focal length cylindrical lens that produced a rectangular spot on the sample. Power densities at the sample were between ≈2 W/cm^2 and ≈9 W/cm^2 for all measurements. The power density was kept relatively low so as to minimize the effects on the spectra of laser-induced heating of the sample and minimize the generation of photoexcited carriers. Spectra obtained with the specified power density were determined to be nominally identical to those obtained with one half the power at the sample, indicating that no sample heating was occurring (within the limit of the instrumental bandpass). Scattered radiation was collected and collimated with an *f*/4 achromatic lens located at infinite conjugate ratio. A dichroic sheet polarizer, holographic notch filter (150 cm^{-1} nominal spectral edgewidth and 6.0 nominal optical density for the respective wavelength), and a bandpass filter were placed in the collected, collimated radiation. The bandpass filter was necessary to limit the wavelength range

of radiation entering the spectrograph so as to reduce interference from reentrant light. The bandpass filter employed with 488 nm and 514.5 nm excitation was optimized for the ≈450 nm to 553 nm wavelength range and possessed a nominal optical density of 5.0 or greater from 553 nm to beyond 1000 nm. The bandpass filter employed with 647.1 nm excitation was optimized for the ≈600 nm to 755 nm wavelength range and possessed a nominal optical density of 5.0 or greater from 755 nm to beyond 1000 nm. The bandpass filter employed with 752.55 nm excitation was optimized for the ≈750 nm to 1100 nm wavelength range and possessed a nominal optical density of greater than 4.5 at wavelengths longer than ≈1140 nm. For 488 nm, 514.5 nm and 647.1 nm excitation, collected radiation was coupled into a single grating, 0.5 m focal length, *f*/6.5 imaging spectrograph using an *f*/7 achromatic lens. For 488 nm and 514.5 nm excitation, a 2400 groove/mm holographic grating optimized for use from 450 nm to 700 nm was utilized and the corresponding instrumental bandpass (FWHM) was approximately 3.0 cm^{-1} and 2.6 cm^{-1} for 488 nm and 514.5 nm excitation, respectively. For 647.1 nm excitation, an 1800 groove/mm ruled grating with a 500 nm blaze wavelength was utilized, unless otherwise specified, in which case a 1200 groove/mm ruled grating with a 500 nm blaze wavelength was utilized. The instrumental bandpass was approximately 2.3 cm^{-1} and 4.1 cm^{-1} for the 1800 groove/mm and 1200 groove/mm grating, respectively. For the 488 nm, 514.5 nm, and 647.1 nm excitation measurements, a thermo-electrically cooled (to -90 °C), 1340 x 400 pixel array (20 μm x 20 μm square pixels), multipin phasing (MPP) back-illuminated charge coupled device (BI CCD) camera system was employed. For 752.55 nm excitation, collected radiation was coupled into a single grating, 0.46 m focal length, *f*/5.3 imaging spectrograph using an *f*/6 achromatic lens. For 752.55 nm excitation, an 1800 groove/mm holographic grating optimized for use from 450 nm to 850 nm was utilized,

unless otherwise specified, in which case a 1200 groove/mm holographic grating with a 750 nm blaze wavelength was utilized. The instrumental bandpass was approximately 1.6 cm^{-1} and 2.9 cm^{-1} for the 1800 groove/mm and 1200 groove/mm grating, respectively. For 752.55 nm excitation, a thermo-electrically cooled (to -90 °C), 1024 x 128 pixel array (26 μm x 26 μm square pixels), deep depletion (DD) BI CCD camera system was employed. While BI CCD camera systems with MPP architecture are preferred for most Raman spectroscopy applications,[25] such detectors suffer from an interference known as etaloning when used at wavelengths longer than ≈700 nm.[26] DD BI CCD camera systems, while somewhat noisier than MPP BI CCD camera systems, [25] can be fabricated so as to eliminate etaloning. Hence, a DD BI CCD camera system was used for this work when 752.55 nm excitation was employed.

All spectra shown represent the average of two spectra, each of which was obtained with a 300 s integration time. For 488 nm, 514.5 nm, and 647.1 nm excitation, atomic lines from an argon pen lamp were used for spectrograph wavelength calibration. For 752.55 nm excitation, atomic lines from an uranium hollow cathode tube were used for wavelength calibration. All Raman scattering intensities were corrected for the wavelength-dependent response of the optical system[27] and by the factor of the square of the wavelength that is required in the transformation of the spectrum abscissa from the measured wavelength (in nanometer) to Raman shift expressed in wavenumber (cm^{-1}).[28] The intensity correction was performed by illuminating a reflecting surface placed at the focal point of the collection lens with a white-light source of known relative irradiance. The white-light source was a 15.2 cm diameter Spectralon integrating sphere (Labsphere[29]) equipped with a 10 W halogen bulb.

RESULTS AND DISCUSSION

N-Type Doped GaSb. GaSb doped n-type exhibits a depletion SSCR.[10,11] To a reasonable approximation, the near-surface region can be described by a two layer model: a depletion SSCR (carriers absent) and the bulk (carriers present).[18] Scattering originating from a depletion SSCR approximates scattering from an undoped bulk crystal and the primary scattering signal originating in the SSCR is that of the longitudinal optic (LO) phonon mode.[4,10,11,30] In GaSb, the LO mode is observed at 236 cm^{-1}. The primary scattering signal originating from the doped bulk is that of the so-called coupled LO phonon-plasmon modes.[4,10,11,30] In n-type GaSb, two coupled phonon-plasmon modes are observed: a low-frequency mode, denoted the L_- mode, and a high-frequency mode, denoted the L_+ mode.[10,11] In the electron concentration ranges investigated in this work, the L_- mode is observed at ≈226 cm^{-1}, while the L_+ mode wavenumber is roughly proportional to (electron concentration)$^{1/2}$ and is observed in the ≈236 cm^{-1} to ≈620 cm^{-1} range.

The n-type epilayers investigated in this work and corresponding DETe mole fraction in the reactor during deposition, Te dopant concentration, N_D, from SIMS measurements, and the Hall effect electron concentration, n_e, and mobility, μ_e, are listed in Table I. Figures 1 to 6 show the Raman spectra of each n-type epilayer excited with 488 nm, 514.5 nm, 647.1 nm, and 752.55 nm excitation. The intensity in each spectrum is normalized to the respective LO phonon mode intensity. For the 647.1 nm and 752.55 nm excitation spectra, the scattering signal in the region of the L_- and LO modes was obtained using an 1800 groove/mm grating while the higher wavenumber scattering signal was obtained using a 1200 groove/mm grating. Comparison of spectra obtained with different gratings is facilitated by normalizing each spectrum to the respective L_- mode intensity (not shown in the higher wavenumber spectrum). Focusing on the

488 nm excitation spectrum for n_e = 4.92 x 10^{17} cm^{-3} (see Fig. 1), the most intense feature is the LO phonon mode scattering from the SSCR (≈236 cm^{-1}). Weak features at ≈226 cm^{-1}, in the ≈265 cm^{-1} to 276 cm^{-1} range, and at ≈440 cm^{-1} are also observed. Nominally identical features are observed in the 488 nm excitation spectrum of the uid-GaSb epilayer (see Fig. 10). Anticipating the discussion of this spectrum, uid-GaSb exhibits no coupled modes that resemble n-GaSb coupled modes. Hence, the weaker common features in the n_e = 4.92 x 10^{17} cm^{-3} and uid-GaSb spectra are attributed to the transverse optic (TO) phonon mode (the feature at ≈226 cm^{-1}) and second order combinational scattering (the features in the ≈265 cm^{-1} to 276 cm^{-1} range and at ≈440 cm^{-1}).[31,32] The TO mode and second order phonon scattering signals originate from the entire probe volume. The TO mode is nominally forbidden in backscattering geometry from the (100) direction and the observation of this mode is attributed to slight deviation of the epilayer from the (100) direction.[4] No bulk scattering is observed in the n_e = 4.92 x 10^{17} cm^{-3} 488 nm excitation spectrum. In contrast, the n_e = 4.92 x 10^{17} cm^{-3} 752.55 nm excitation spectrum exhibits relatively intense bulk coupled mode features: the L_- mode at ≈226 cm^{-1} and the L_+ mode in the ≈236 cm^{-1} to 400 cm^{-1} range (see Fig. 1). Since the SSCR width is nominally the same in all spectra, the change in bulk scattering intensity relative to SSCR scattering intensity is attributed to a change in Raman probe depth with excitation wavelength. The Raman probe depth, d_{RP}, is given by:

$$d_{RP} = 1/(\alpha_I + \alpha_S) \tag{1}$$

where α_I and α_S are the absorption coefficients of the incident and scattered radiation, respectively. As absorption coefficient decreases with increasing wavelength,[6] d_{RP} increases such that d_{RP} for 752.55 nm radiation is approximately twice d_{RP} for 647.1 nm radiation and approximately 7 to 8 times d_{RP} for 488 nm and 514.5 nm radiation.

It is apparent from Figures 1 to 6 that the bulk coupled mode-to-SSCR scattering intensity ratio is dependent on both excitation wavelength and carrier concentration. In general, the bulk coupled mode-to-SSCR scattering intensity ratio increases with increasing excitation wavelength and n_e, as expected since Raman probe depth increases with increasing wavelength and SSCR width generally decreases with increasing electron concentration. These trends can be used to estimate the SSCR width, d_{dep}, using a relatively simple model in which a two layer system with an abrupt junction is assumed:[10,16]

$$\frac{I_{L_-}}{I_{LO}} = \frac{I^0_{L_-}}{I^0_{LO}} \frac{\exp\left(-\left(\alpha_I + \alpha_S\right)d_{dep}\right)}{\exp\left(1 - \left(\alpha_I + \alpha_S\right)d_{dep}\right)} \tag{2}$$

where I_{L_-} and I_{LO} are the intensities of the L_- (the L_- mode was selected since it is more intense than the L_+ mode) and LO modes, respectively, $I^0_{L_-}$ is the I_{L_-} mode intensity in an epilayer without a SSCR, and I^0_{LO} is the I_{LO} mode intensity in an undoped epilayer. The values of $\left(I_{L_-}/I_{LO}\right)\left(I^0_{LO}/I^0_{L_-}\right)$ for all spectra shown in Figures 1 to 6 are plotted as a function of excitation wavelength in Fig. 7. For each n-type epilayer listed in Table I, a value of d_{dep} was determined by fitting Eq. 2 to the corresponding $\left(I_{L_-}/I_{LO}\right)\left(I^0_{LO}/I^0_{L_-}\right)$ values as a function of wavelength (see Fig. 7) and using d_{dep} as the fit parameter. For each spectrum, the I_{L_-} value was determined by subtracting the TO phonon intensity for the uid-GaSb observed at the corresponding excitation wavelength (see Fig. 10) from the intensity of the ≈226 cm^{-1} feature in Figures 1 to 6. Values for $I^0_{L_-}$ are best obtained from spectra of SSCR-free epilayers. However, no such epilayers existed. Therefore, for each wavelength, the value for $I^0_{L_-}$ was taken from the L_- mode intensity value in the spectra of the epilayer with the smallest SSCR width (epilayers

grown with a DETe mole fraction of 50 x 10^{-9}). Although these epilayers were not SSCR-free, the plot of all L_- mode intensity values as a function of DETe mole fraction asymptotically approached an intensity value close to that observed in the spectra of these epilayers. Values for I_{LO}^{0} are best obtained from spectra of undoped epilayers. However, uid-GaSb is lightly p-type and exhibits an accumulation SSCR, holes in which can modify the observed LO phonon mode spectrum (see Fig. 10 and associated discussion). For the 647.1 nm and 752.55 nm excitation spectra, it was determined that the effects of holes in the accumulation SSCR on the uid-GaSb spectrum were small and the value of I_{LO}^{0} was obtained from the LO phonon mode intensity in the uid-GaSb epilayer (see Fig. 10 and associated discussion). However, for the 488 nm and 514.5 nm excitation spectra, it was determined that the effects of the accumulation SSCR on the uid-GaSb spectrum were not small. Hence, the value of I_{LO}^{0} was obtained from the LO phonon mode intensity in the spectra of the epilayers with the largest SSCR width (epilayers grown with a DETe mole fraction of 5 x 10^{-9}). Although the spectra of these epilayers were not free of bulk coupled mode scattering and the corresponding I_{LO}^{0} values are probably correspondingly low, the L_- mode intensity was vanishingly small in the 488 nm and 514.5 nm excitation spectra and, consequently, the $\left(I_{\mathrm{L}_-}/I_{\mathrm{LO}}\right)\left(I_{\mathrm{LO}}^{0}/I_{\mathrm{L}_-}^{0}\right)$ values were not greatly influenced by the I_{LO}^{0} value. In general, the fit was not greatly influenced by the absolute values of $\left(I_{\mathrm{L}_-}/I_{\mathrm{LO}}\right)\left(I_{\mathrm{LO}}^{0}/I_{\mathrm{L}_-}^{0}\right)$ at 488 nm and 514.5 nm. The nominal d_{dep} values obtained from the fits are listed in Table II. From the d_{dep} and N_{D} values, the value of the surface band-bending potential, V_{S}, can be estimated using a simple expression for an abrupt junction:[16,18]

$$d_{\mathrm{dep}} \cong \sqrt{2\varepsilon_{\mathrm{s}}\varepsilon_{0}|V_{\mathrm{S}}|/eN_{\mathrm{D}}} \tag{3}$$

where ε_S is the static dielectric constant, ε_0 is the electric constant, and e is the elementary charge. Assuming complete ionization of the dopants and no significant compensation and using the d_{dep} values in Table II, the N_D values in Table I, and $\varepsilon_S = 15.7$,[33] V_S values in the range from ≈0.5 eV to ≈0.8 eV were calculated. This range is in reasonable agreement with the value of 0.4 eV reported by Kauschke, et al.[10]

The estimated d_{dep} values are plotted as a function of n_e and compared to the Raman probe depth as a function of wavelength in Fig. 8. The Raman probe depth was calculated for Raman shifts ranging from 0 cm^{-1} to 1000 cm^{-1} (a wavenumber range spanning the observed coupled mode wavenumber range) relative to Raman scattering excitation wavelengths of 488 nm, 514.5 nm, 647.1 nm, and 752.55 nm (solid lines) using Eq. 1 and a range of corresponding α_S values as reported by Muñoz et al.[6] In Fig. 8, Raman probe depth is plotted to help illustrate trends and is not meant to indicate the depth limit from which signal is detected. Raman probe depth is defined in Eq. 1 in terms of the intensity of scattered radiation that escapes from the optical probe depth. In an absorbing medium, the optical probe depth is defined as the depth at which the intensity of radiation has decreased to 1/e times the intensity of the incident radiation at the surface.[34] Hence, it is possible to detect scattered radiation originating from deeper than the Raman probe depth for a sufficiently high incident intensity (as is apparent from the spectra). Further, different incident laser power levels were used for different excitation wavelengths. Therefore, the difference between the depth from which signal is detected and the Raman probe depth is expected to vary with excitation wavelength. However, by examining the relative contributions from SSCR and bulk scattering, the effects of differences in defined probe depth to actual probe depth are eliminated. It is apparent from Figures 1 to 8 that the observed Raman scattering with 488 nm excitation includes a large component originating in the SSCR,

especially for epilayers with lower n_e (larger d_{dep}). All observed scattering in the lowest n_e epilayer 488 nm excitation spectrum is attributed to SSCR scattering (see Fig. 1). Even for higher n_e, the only difference in spectra is a small increase in scattering intensity and peak FWHM at ≈226 cm^{-1}, attributed to increased L_- mode scattering. Spectra excited with 514.5 nm radiation also exhibit little bulk scattering. The L_- mode signal is slightly more pronounced in the 514.5 nm excitation spectra than in the 488 nm excitation spectra, but the signal is still weak. For the laser intensity employed here, no L_+ mode signal is observed in any spectrum excited with 488 nm or 514.5 nm radiation. While both of the coupled modes become more pronounced in the spectra excited with 647.1 nm excitation spectra compared to the spectra excited with the two shorter wavelengths, the bulk-to-SSCR scattering signal ratio is still low. In contrast, spectra excited with 752.55 nm radiation show a relatively intense bulk-to-SSCR scattering signal ratio across the whole n_e range investigated in this work.

P-Type Doped GaSb. GaSb doped p-type exhibits a hole accumulation SSCR.[7-9,35] Unlike n-type GaSb, a two-layer model is a poor approximation of the surface region and a three-layer model is often used to describe this system.[17,18] Moving from a point in the interior of the layer towards the surface, the three layers correspond to the bulk with a given hole concentration, a layer between the surface and the bulk that is enriched in hole concentration relative to the bulk, and a surface layer of zero hole concentration. In this three layer model and employing scattering excitation of sufficient optical penetration depth to probe the bulk, LO phonon-hole plasmon coupled mode scattering originates from both the bulk and the hole-enriched layer and LO phonon mode scattering originates from the hole-depleted near-surface layer. Few reports on experimental or theoretical p-type GaSb coupled mode Raman spectra exist. In the limited number of Raman spectroscopic investigations of p-type GaSb accumulation

layer spectra reported, the accumulation SSCR coupled mode is observed at a slightly lower wavenumber and is broadened with respect to the LO phonon mode.[7-9] Although, to these authors' knowledge, no systematic report of bulk GaSb bulk hole coupled mode spectra has been reported, the general characteristics can be deduced by analogy to p-type GaAs, for which a number of reports exist.[36-39] Briefly summarizing the trends observed for the coupled modes originating in the bulk of p-type GaAs, at low hole concentrations, one coupled mode is observed with a linewidth and peak wavenumber that are very similar to those of the LO phonon mode. As the hole concentration increases, the bulk coupled mode linewidth broadens with respect to that of the LO phonon mode. Also as the hole concentration increases, the bulk coupled mode peak wavenumber first increases from nearly that of the LO phonon mode (but by no more than ≈ 2 cm^{-1}) and then starts to decrease and approaches the TO phonon wavenumber. At higher hole concentrations, it is expected that two coupled modes may be observed.[38] However, to these authors' knowledge, observation of the higher frequency coupled mode has not been reported.

Assuming that the coupled mode dependence on n_p of bulk p-GaSb is qualitatively the same as that of bulk p-GaAs, it is expected that the bulk and SSCR coupled modes will be observed at nearly identical wavenumber over a large n_p range, thereby making the resolution of scattering from the bulk and SSCR difficult. This similarity in bulk and SSCR mode spectra precludes the experimental determination of the SSCR width, e.g., based on Eq. 2. Theoretical determination of SSCR width employing quantum mechanical methods is beyond the scope of this article, however some SSCR width estimates have been reported in the literature. Although the method of determination was not explained in detail in all reports, accumulation layer widths in p-GaSb have been reported to be ≈ 15 nm, ≈ 8 nm, ≈ 5 nm, and ≈ 2 nm for bulk hole densities of 4×10^{16} cm^{-3},[8] 1.4×10^{17} cm^{-3},[35] 2.3×10^{17} cm^{-3},[9] and 4×10^{18} cm^{-3},[7] respectively. These

reported values are plotted in Fig. 9 as a function of hole concentration. Also shown as an aid to the eye is an approximation for the accumulation layer thickness, d_{acc}, as a function of hole density (dashed-dotted line) based on the simplified expression:[18]

$$d_{acc} \cong \frac{\left(2\varepsilon_s\varepsilon_0 k_B T / e^2 p\right)^{1/2} |V_S / k_B T|}{\left[2\left(\exp|V_S / k_B T| - |V_S / k_B T| - 1\right)\right]^{1/2}} \tag{4}$$

where p is the bulk hole density, k_B is the Boltzmann constant, and T is the thermodynamic temperature. The curve plotted in Fig. 9 was created by fitting Eq. 4 to the reported d_{acc} values as a function of hole concentration and using V_S as the fit parameter (V_S = 0.097 eV resulted in the best fit and was used in Fig. 9). Also plotted in Fig. 9 is the Raman probe depth as a function of wavelength, calculated as using Eq. 1 (also shown in Fig. 8).

The p-type epilayers investigated in this work and corresponding DMZn mole fraction in the reactor during deposition and the Hall effect hole concentration, n_p, and mobility, μ_p, are listed in Table III. Figures 10 to 14 show the Raman spectra of each p-type epilayer excited with 488 nm, 514.5 nm, 647.1 nm, and 752.55 nm excitation. The intensity in each spectrum is normalized to the most intense feature in the respective spectrum. To aid in the identification of observed trends relative to the uid-GaSb spectra, the positions of the most intense feature in the 488 nm and 752.55 nm excitation uid-GaSb spectra (see Fig. 10) are indicated by the two vertical lines in Figures 10 to 14. The difference in linewidths between spectra obtained with different excitation wavelengths is attributed to the decrease in instrumental bandwidth with increasing excitation wavelength (see **Raman Spectroscopic Measurements** section).

Based on the trends observed in the spectra and the relationships summarized in Fig. 9 (assuming that the boundary conditions for the reported models apply to the materials investigated in this work), a number of conclusions can be drawn about the relative contributions

to the overall spectra from bulk, hole-enriched SSCR, and hole-depleted SSCR scattering. For the 752.55 nm excitation spectra of epilayers with n_p = 1.92 x 10^{17} cm^{-3} to 1.14 x 10^{18} cm^{-3}, only one intense feature is observed. The wavenumber of this features shifts from the uid-GaSb LO phonon mode wavenumber to higher wavenumber with increasing n_p in these spectra. These trends are consistent with those observed in Raman spectra of p-type GaAs. For the epilayer with a n_p = 6.38 x 10^{18} cm^{-3} (see Fig. 14), the coupled mode spectrum consists of two features: a relatively intense, broad mode near the TO phonon mode wavenumber and a weaker, broader mode in the ≈250 cm^{-1} to 500 cm^{-1} range (not fully shown). The observation of the most intense feature near the TO phonon wavenumber is consistent with the characteristics of highly doped p-type GaAs Raman spectra. The observation of the second coupled mode is inconsistent with experimental results for p-type GaAs. The reason for the observation of the high frequency mode in this work is not known. Possible reasons for this observation may be the intrinsic properties of the two materials and/or the relative material quality between the highly doped GaSb investigated here and highly doped GaAs investigated in published reports. A feature is also observed in the n_p = 6.38 x 10^{18} cm^{-3} near the LO phonon mode wavenumber. This feature is attributed to scattering from the hole-depleted and/or hole-enriched region of the accumulation SSCR. Although the signal-to-noise ratio of this spectrum is relatively poor, this feature is broad and could be composed of at least two peaks: one with a wavenumber near that of the uid-GaSb LO mode wavenumber and one with a wavenumber lower than the uid-GaSb LO mode wavenumber. A peak at the uid-GaSb LO mode wavenumber would be attributed to scattering from the hole-depleted SSCR. A peak with a lower wavenumber than the the uid-GaSb LO mode wavenumber would be consistent with scattering from a coupled mode in the hole-enriched region.[7-9] Presumably, this feature is present in the spectra of the other epilayers but is

not resolved (although a weak shoulder is observed at this wavenumber in the n_p = 1.14 x 10^{18} cm^{-3} epilayer spectrum) because of the similarity between the bulk and SSCR coupled mode wavenumbers (in contrast to the n_p = 6.38 x 10^{18} cm^{-3} spectrum). For 752.55 nm excitation, the consistency of the GaSb spectral trends with those of bulk p-type GaAs coupled mode spectra and the large Raman probe depth relative to the SSCR width, indicates that the observed scattering signal originates primarily in the bulk for all epilayers, although SSCR scattering is observed in the spectra of the (weakly) n_p = 1.14 x 10^{18} cm^{-3} and n_p = 6.38 x 10^{18} cm^{-3} epilayers for which bulk and SSCR modes are spectrally resolved and d_{acc} is relatively thin.

Similar trends to the 752.55 nm excitation spectra are observed in the 647.1 nm excitation spectra, although SSCR scattering is somewhat more intense. For example, the n_p = 1.14 x 10^{18} cm^{-3} and 6.38 x 10^{18} cm^{-3} epilayer spectra excited with 647.1 nm exhibit a more intense shoulder in the LO phonon mode wavenumber range (see Figures 13 and 14), indicating a larger contribution from SSCR scattering in the case of the 647.1 nm excitation spectrum compared to the 752.55 nm excitation spectrum.

The 488 nm excitation spectra of the n_p = 1.92 x 10^{17} cm^{-3} to 1.14 x 10^{18} cm^{-3} epilayers exhibit an intense feature that decreases in wavenumber with increasing n_p and a shoulder that becomes more readily apparent at ≈225 cm^{-1} to 235 cm^{-1} in the n_p = 5.51 x 10^{17} cm^{-3} and 1.14 x 10^{18} cm^{-3} epilayer spectra. The decrease in wavenumber of the most intense feature in these spectra is opposite of the shift observed for the 647.1 nm and 752.55 nm excitation spectra. The inconsistency of this trend with observed bulk coupled mode characteristics, the similarity to reported SSCR scattering, and the small Raman probe depth of 488 nm excitation relative to the SSCR width, indicates that SSCR scattering is responsible for this trend. The shoulder observed

at higher wavenumber is attributed to bulk coupled mode scattering by comparison to the 647.1 nm and 752.55 nm excitation spectra. The 488 nm excitation spectrum of the n_p = 6.38 x 10^{18} cm^{-3} epilayer is similar to the 647.1 nm and 752.55 nm excitation spectra, although there are some differences. The SSCR scattering intensity (the feature near the uid-GaSb LO mode wavenumber) relative to the bulk scattering intensity (the feature near the TO mode wavenumber) is higher in the 488 nm excitation spectrum compared to the 647.1 nm and 752.55 nm excitation spectra. The SSCR scattering feature is at a lower wavenumber than the uid-GaSb LO mode but exhibits a weak shoulder near the uid-GaSb LO mode wavenumber, indicating that scattering from the SSCR coupled mode and SSCR LO mode probably contribute to the observed signal. In contrast to the 647.1 nm and 752.55 nm excitation spectra, the 488 nm excitation spectrum of the n_p = 6.38 x 10^{18} cm^{-3} epilayer does not exhibit the second bulk coupled mode (in the ≈250 cm^{-1} to 500 cm^{-1} range). This is attributed to the decreased Raman probe depth for these excitation wavelengths and a relatively small scattering efficiency of this plasmon-like coupled mode. The 514.5 nm excitation spectra exhibit a combination of the longer-excitation wavelength and shorter-excitation wavelength trends, although the spectra most closely resemble the 488 nm excitation spectra.

CONCLUSION

Raman spectra of both n-type and p-type doped GaSb epilayers, exhibiting a range of SSCR profiles, were obtained using 488 nm, 514.5 nm, 647.1 nm, and 752.55 nm excitation radiation. For n-type epilayers, the SSCR width was determined from the bulk-to-SSCR scattering intensity ratios in the experimental spectra. For p-type epilayers, the SSCR width as a function of hole concentration was estimated from literature reports. Comparisons of the SSCR width to Raman probe depth aided in the determination of the relative contributions to overall

scattering signal of scattering originating in the SSCR and bulk. For both n-type and p-type GaSb, spectra excited with 752.55 nm radiation showed relatively high bulk-to-SSCR scattering intensity ratios across the whole n_e range investigated in this work. In contrast, spectra excited with 488 nm radiation showed low bulk-to-SSCR scattering intensity ratios across the whole n_e range investigated in this work. Hence, for GaSb with the doping types and carrier concentration ranges and the common ion laser wavelengths employed here, SSCR properties are best probed with 488 nm radiation and bulk properties are best probed with 752.55 nm radiation.

ACKNOWLEDGMENTS

The authors gratefully acknowledge D. A. Shiau for assistance in the growth of epilayers and in the performance of the single magnetic field Hall effect measurements and M. Muñoz for GaSb spectroscopic ellipsometric data.

REFERENCES

1. A. Aardvark, N. J. Mason, and P. J. Walker, Progress in Crystal Growth and Characterization of Materials **35,** 207 (1997).
2. R. M. Biefeld, Materials Science & Engineering R-Reports **36,** 105 (2002).
3. P. S. Dutta, H. L. Bhat, and V. Kumar, J. Appl. Phys. **81,** 5821 (1997).
4. G. Abstreiter, E. Bauser, A. Fischer, and K. Ploog, Applied Physics **16,** 345 (1978).
5. W. Mönch, in *Semiconductor Surfaces and Interfaces* (Springer-Verlag, Berlin, 1993), p. 12.
6. M. Muñoz, K. Wei, F. H. Pollak, J. L. Freeouf, and G. W. Charache, Phys. Rev. B **60,** 8105 (1999).
7. R. Dornhaus, R. L. Farrow, and R. K. Chang, Solid State Commun. **35,** 123 (1980).
8. R. Dornhaus, R. L. Farrow, R. K. Chang, and R. M. Martin, in *Light Scattering in Solids*, edited by J. L. Birman, H. Z. Cummins, and K. K. Rebane (Plenum Press, New York, 1979), p. 299.
9. R. L. Farrow, R. K. Chang, and R. M. Martin; *Vol. Physics of Semiconductors, Conference Series Vol. 43*, edited by B. L. H. Wilson (Institute of Physics, Edinburgh, 1979), p. 485.
10. W. Kauschke, N. Mestres, and M. Cardona, Phys. Rev. B **36,** 7469 (1987).
11. R. Trommer and A. K. Ramdas, in *Physics of Semiconductors, 1978*; *Vol. 43*, edited by B. L. H. Wilson (Institute of Physics, Edinburgh, 1979), p. 585.
12. H. S. Bennett, H. Hung, and A. Heckert, J. Appl. Phys. **98** (2005).
13. I. M. J. R. R.-M. L. R. Vurgaftman, J. Appl. Phys. **89,** 5815 (2001).

14. B. C. Dodrill, J. R. Lindemuth, B. J. Kelley, G. Du, and J. R. Meyer, Compound Semiconductor **7,** 58 (2001).

15. C. Pickering, Journal of Physics C-Solid State Physics **13,** 2959 (1980).

16. J. Geurts, Surface Science Reports **18,** 1 (1993).

17. G. R. Bell, C. F. McConville, and T. S. Jones, Phys. Rev. B **54,** 2654 (1996).

18. W. Mönch, in *Semiconductor Surfaces and Interfaces* (Springer-Verlag, Berlin, 1993), p. 19.

19. C. A. Wang, J. Cryst. Growth **191,** 631 (1998).

20. C. A. Wang, D. A. Shiau, R. K. Huang, C. T. Harris, and M. K. Connors, J. Cryst. Growth **261,** 379 (2004).

21. M. W. Heller and R. G. Hamerly, J. Appl. Phys. **57,** 4626 (1985).

22. P. C. Mathur and S. Jain, Phys. Rev. B **19,** 3152 (1979).

23. C. D. Kourkoutas, P. D. Bekris, G. J. Papaioannou, and P. C. Euthymiou, Solid State Commun. **49,** 1071 (1984).

24. R.-Y. Sun and W. M. Becker, Phys. Rev. B **10,** 3436 (1974).

25. J. B. Slater, J. M. Tedesco, R. C. Fairchild, I. R. Lewis, I. R. Lewis, and H. G. M. Edwards, in *Handbook of Raman Spectroscopy From the Research Laboratory to the Process Line* (Marcel Dekker, Inc., New York, 2001), p. 41.

26. R. L. McCreery, in *Raman spectroscopy for chemical analysis*, edited by J. D. Winefordner (John Wiley & Sons, Inc., New York, 2000), p. 149.

27. M. Fryling, C. J. Frank, and R. L. McCreery, Appl. Spectrosc. **47,** 1965 (1993).

28. K. J. Frost and R. L. McCreery, Appl. Spectrosc. **52,** 1614 (1998).

29. Certain commercial equipment, instruments, and materials are identified in this publication to adequately specify the experimental procedure. Such identification in no way implies approval, recommendation, or endorsement by the National Institute of Standards and Technology, nor does it imply that the equipment, instruments, or materials identified are necessarily the best available for the purpose.

30. G. Abstreiter, M. Cardona, and A. Pinczuk, in *Topics in Applied Physics*; *Vol. 54* (1984), p. 5.

31. P. B. Klein and R. K. Chang, Phys. Rev. B **14,** 2498 (1976).

32. T. Sekine, K. Uchinokura, and E. Matsuura, Solid State Commun. **18,** 1337 (1976).

33. A. Y. Vul', M. E. Levinshtein, S. L. Rumyantsev, and M. S. Shur, in *Handbook Series on Semiconductor Parameters: Vol. 1, Si, Ge, C (Diamond), GaAs, GaP, GaSb, InAs, InP, InSb* (World Scientific Publishing Co., Singapore, 1996), p. 125.

34. H. G. Tompkins, in *A User's Guide to Ellipsometry* (Academic Press, Inc., San Diego, CA, 1993), p. 1.

35. J. P. Nerou, A. Filion, and P. E. Girard, Journal of Physics C-Solid State Physics **9,** 479 (1976).

36. R. Fukasawa and S. Perkowitz, Phys. Rev. B **50,** 14119 (1994).

37. G. Irmer, M. Wenzel, and J. Monecke, Phys. Rev. B **56,** 9524 (1997).

38. K. Wan and J. F. Young, Phys. Rev. B **41,** 10772 (1990).

39. T. Yuasa and M. Ishii, Phys. Rev. B **35,** 3962 (1987).

Table I. The n-type epilayers investigated in this work and corresponding DETe mole fraction in the reactor during deposition, Te dopant concentration, N_D, as determined from SIMS measurements, and electron concentration, n_e, and mobility, μ_e, as determined from single magnetic field Hall effect measurements.

DETe Mole Fraction	N_D (cm^{-3})	n_e (cm^{-3})	μ_e (cm^2/V-s)
5.0×10^{-9}	1.53×10^{18}	4.92×10^{17}	3179
7.5×10^{-9}		6.48×10^{17}	2736
10×10^{-9}	3.26×10^{18}	7.40×10^{17}	2526
15×10^{-9}		8.82×10^{17}	2259
25×10^{-9}	7.18×10^{18}	1.04×10^{18}	1927
50×10^{-9}	1.50×10^{19}	1.17×10^{18}	1650

Table II. The nominal d_{dep} values obtained from a fit of Eq. (2) to the $\left(I_{L_-}/I_{LO}\right)\left(I^0_{LO}/I^0_{L_-}\right)$ values plotted in Fig. 7 for n-type GaSb epilayers.

n_e (cm^{-3})	d_{dep} (nm)
4.92×10^{17}	26
6.48×10^{17}	19
7.40×10^{17}	16
8.82×10^{17}	13
1.04×10^{18}	12
1.17×10^{18}	10

Table III. The p-type epilayers investigated in this work and corresponding DMZn mole fraction in the reactor during deposition and hole concentration, n_p, and mobility, μ_p, as determined from single magnetic field Hall effect measurements.

DMZn Mole Fraction	n_p (cm^{-3})	μ_p (cm^2/V-s)
0	1.44×10^{16}	804
1×10^{-6}	1.92×10^{17}	677
2×10^{-6}	5.51×10^{17}	570
4×10^{-6}	1.14×10^{18}	477
10×10^{-6}	6.38×10^{18}	290

FIGURE CAPTIONS

Figure 1. The Raman spectra of the n_e = 4.92 x 10^{17} cm^{-3} epilayer excited with 488 nm, 514.5 nm, 647.1 nm, and 752.55 nm excitation. The intensity in each spectrum is normalized to the respective LO phonon mode intensity and the spectra are offset on the intensity scale.

Figure 2. The Raman spectra of the n_e = 6.48 x 10^{17} cm^{-3} epilayer excited with 488 nm, 514.5 nm, 647.1 nm, and 752.55 nm excitation. The intensity in each spectrum is normalized to the respective LO phonon mode intensity and the spectra are offset on the intensity scale.

Figure 3. The Raman spectra of the n_e = 7.40 x 10^{17} cm^{-3} epilayer excited with 488 nm, 514.5 nm, 647.1 nm, and 752.55 nm excitation. The intensity in each spectrum is normalized to the respective LO phonon mode intensity and the spectra are offset on the intensity scale.

Figure 4. The Raman spectra of the n_e = 8.82 x 10^{17} cm^{-3} epilayer excited with 488 nm, 514.5 nm, 647.1 nm, and 752.55 nm excitation. The intensity in each spectrum is normalized to the respective LO phonon mode intensity and the spectra are offset on the intensity scale.

Figure 5. The Raman spectra of the n_e = 1.04 x 10^{18} cm^{-3} epilayer excited with 488 nm, 514.5 nm, 647.1 nm, and 752.55 nm excitation. The intensity in each spectrum is normalized to the respective LO phonon mode intensity and the spectra are offset on the intensity scale.

Figure 6. The Raman spectra of the n_e = 1.17 x 10^{18} cm^{-3} epilayer excited with 488 nm, 514.5 nm, 647.1 nm, and 752.55 nm excitation. The intensity in each spectrum is normalized to the respective LO phonon mode intensity and the spectra are offset on the intensity scale.

Figure 7. The $\left(I_{L_-}/I_{LO}\right)\left(I^0_{LO}/I^0_{L_-}\right)$ values for all spectra shown in Figures 1 to 6 plotted as a function of excitation wavelength.

Figure 8. The depletion SSCR widths determined using Eq. 2 plotted as a function of n_e for the n-type GaSb epilayers (●) and compared to the Raman probe depth as a function of wavelength

for Raman shifts ranging from 0 cm^{-1} to 1000 cm^{-1} relative to Raman scattering excitation wavelengths of 488 nm, 514.5 nm, 647.1 nm, and 752.55 nm using Eq. 1 (solid lines).

Figure 9. The reported accumulation SSCR widths for the p-type GaSb as a function of n_p (●) and compared to the Raman probe depth as a function of wavelength for Raman shifts ranging from 0 cm^{-1} to 1000 cm^{-1} relative to Raman scattering excitation wavelengths of 488 nm, 514.5 nm, 647.1 nm, and 752.55 nm using Eq. 1 (solid lines). Shown as an aid to the eye is the SSCR width as a function of hole density approximated using Eq. 4 with V_S = 0.097 eV (dashed-dotted line).

Figure 10. The Raman spectra of the n_p = 1.44 x 10^{16} cm^{-3} epilayer excited with 488 nm, 514.5 nm, 647.1 nm, and 752.55 nm excitation. The intensity in each spectrum is normalized to the most intense feature in the respective spectrum and the spectra are offset on the intensity scale. The two vertical lines indicate the positions of the most intense feature in the 488 nm and 752.55 nm excitation uid-GaSb spectra (see Fig. 10).

Figure 11. The Raman spectra of the n_p = 1.92 x 10^{17} cm^{-3} epilayer excited with 488 nm, 514.5 nm, 647.1 nm, and 752.55 nm excitation. The intensity in each spectrum is normalized to the most intense feature in the respective spectrum and the spectra are offset on the intensity scale. The two vertical lines indicate the positions of the most intense feature in the 488 nm and 752.55 nm excitation uid-GaSb spectra (see Fig. 10).

Figure 12. The Raman spectra of the n_p = 5.51 x 10^{17} cm^{-3} epilayer excited with 488 nm, 514.5 nm, 647.1 nm, and 752.55 nm excitation. The intensity in each spectrum is normalized to the most intense feature in the respective spectrum and the spectra are offset on the intensity scale. The two vertical lines indicate the positions of the most intense feature in the 488 nm and 752.55 nm excitation uid-GaSb spectra (see Fig. 10).

Figure 13. The Raman spectra of the n_p = 1.14 x 10^{18} cm^{-3} epilayer excited with 488 nm, 514.5 nm, 647.1 nm, and 752.55 nm excitation. The intensity in each spectrum is normalized to the most intense feature in the respective spectrum and the spectra are offset on the intensity scale. The two vertical lines indicate the positions of the most intense feature in the 488 nm and 752.55 nm excitation uid-GaSb spectra (see Fig. 10).

Figure 14. The Raman spectra of the n_p = 6.38 x 10^{18} cm^{-3} epilayer excited with 488 nm, 514.5 nm, 647.1 nm, and 752.55 nm excitation. The intensity in each spectrum is normalized to the most intense feature in the respective spectrum and the spectra are offset on the intensity scale. The two vertical lines indicate the positions of the most intense feature in the 488 nm and 752.55 nm excitation uid-GaSb spectra (see Fig. 10).

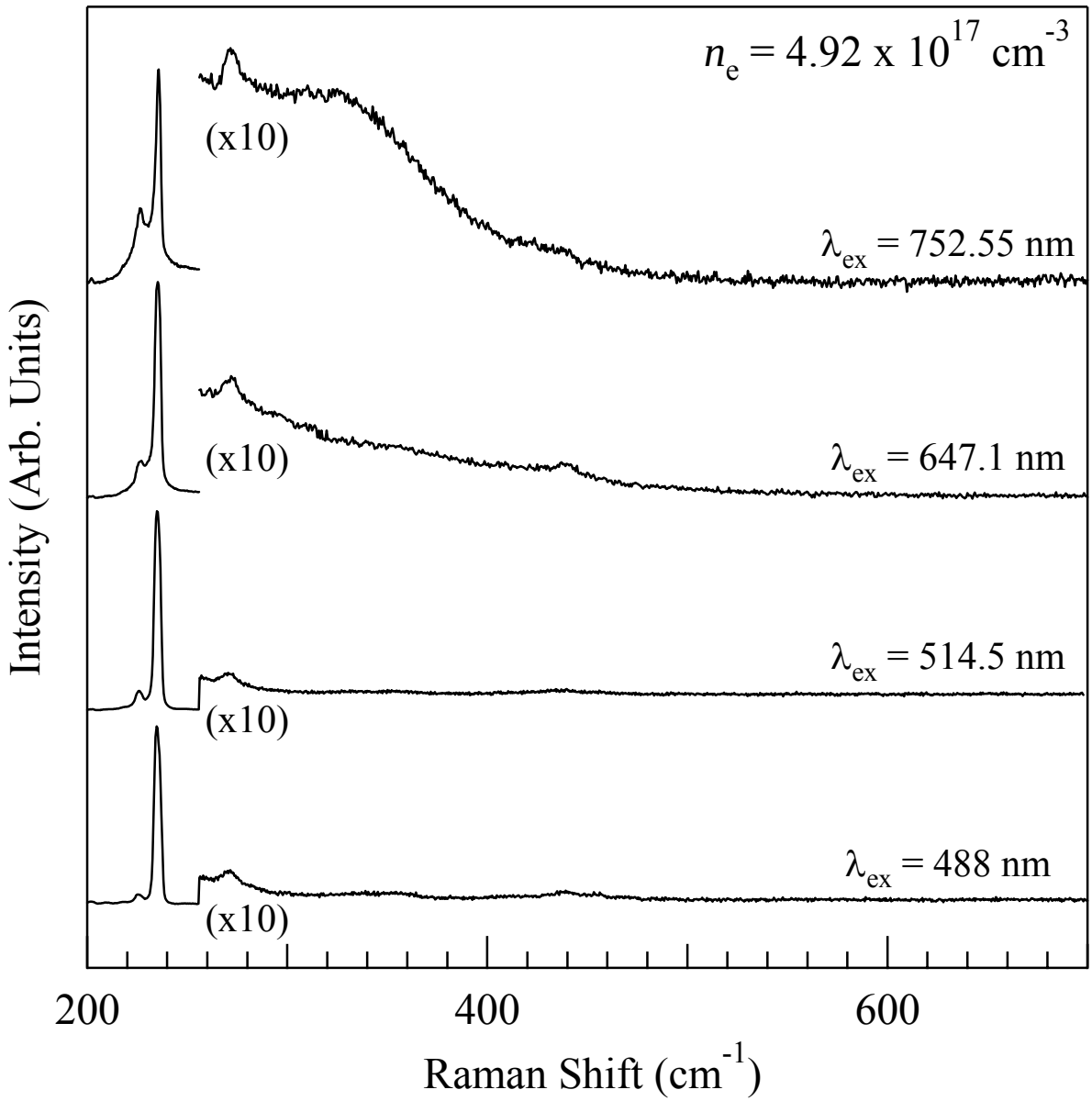
n_e = 4.92 x 10^{17} cm^{-3}
(x10)
λ_{ex} = 752.55 nm
(x10)
λ_{ex} = 647.1 nm
λ_{ex} = 514.5 nm
(x10)
λ_{ex} = 488 nm
(x10)
Intensity (Arb. Units)
200
400
600
Raman Shift (cm^{-1})

Figure 1

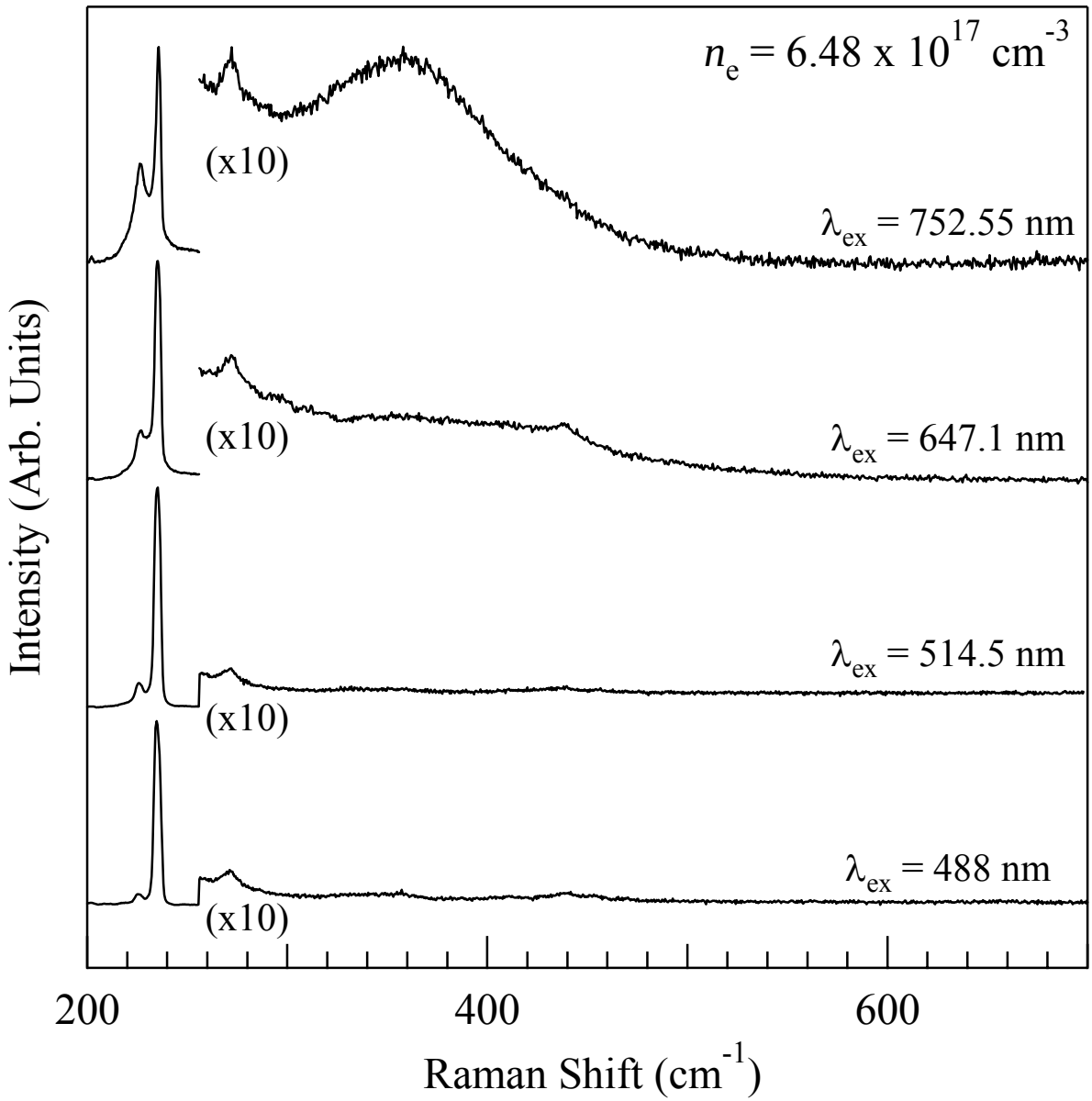
n_e = 6.48 x 10^{17} cm^{-3}
(x10)
λ_{ex} = 752.55 nm
(x10)
λ_{ex} = 647.1 nm
λ_{ex} = 514.5 nm
(x10)
λ_{ex} = 488 nm
(x10)
Intensity (Arb. Units)
200
400
600
Raman Shift (cm^{-1})

Figure 2

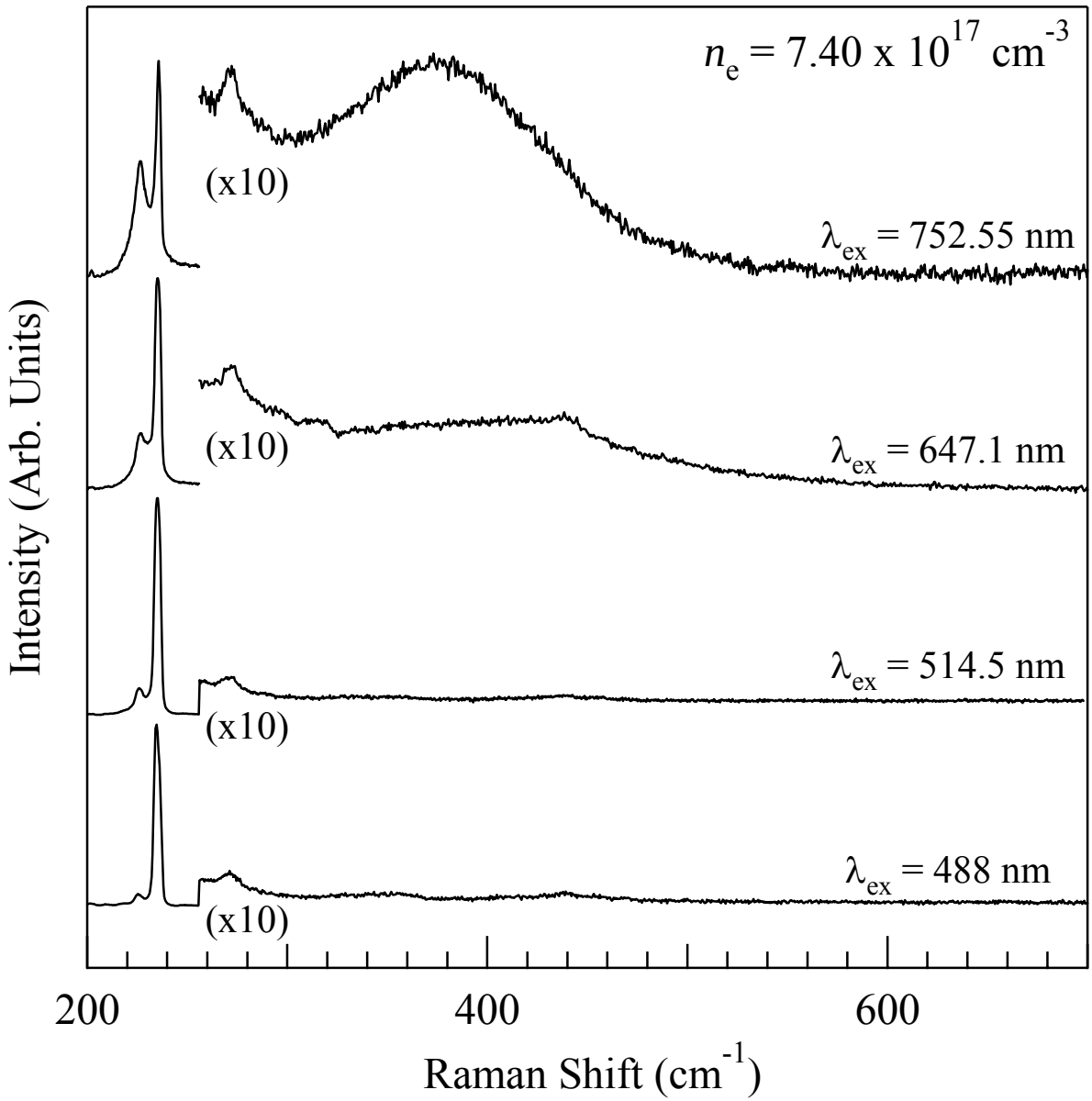
n_e = 7.40 x 10^{17} cm^{-3}
(x10)
λ_{ex} = 752.55 nm
(x10)
λ_{ex} = 647.1 nm
λ_{ex} = 514.5 nm
(x10)
λ_{ex} = 488 nm
(x10)
Intensity (Arb. Units)
200
400
600
Raman Shift (cm^{-1})

Figure 3

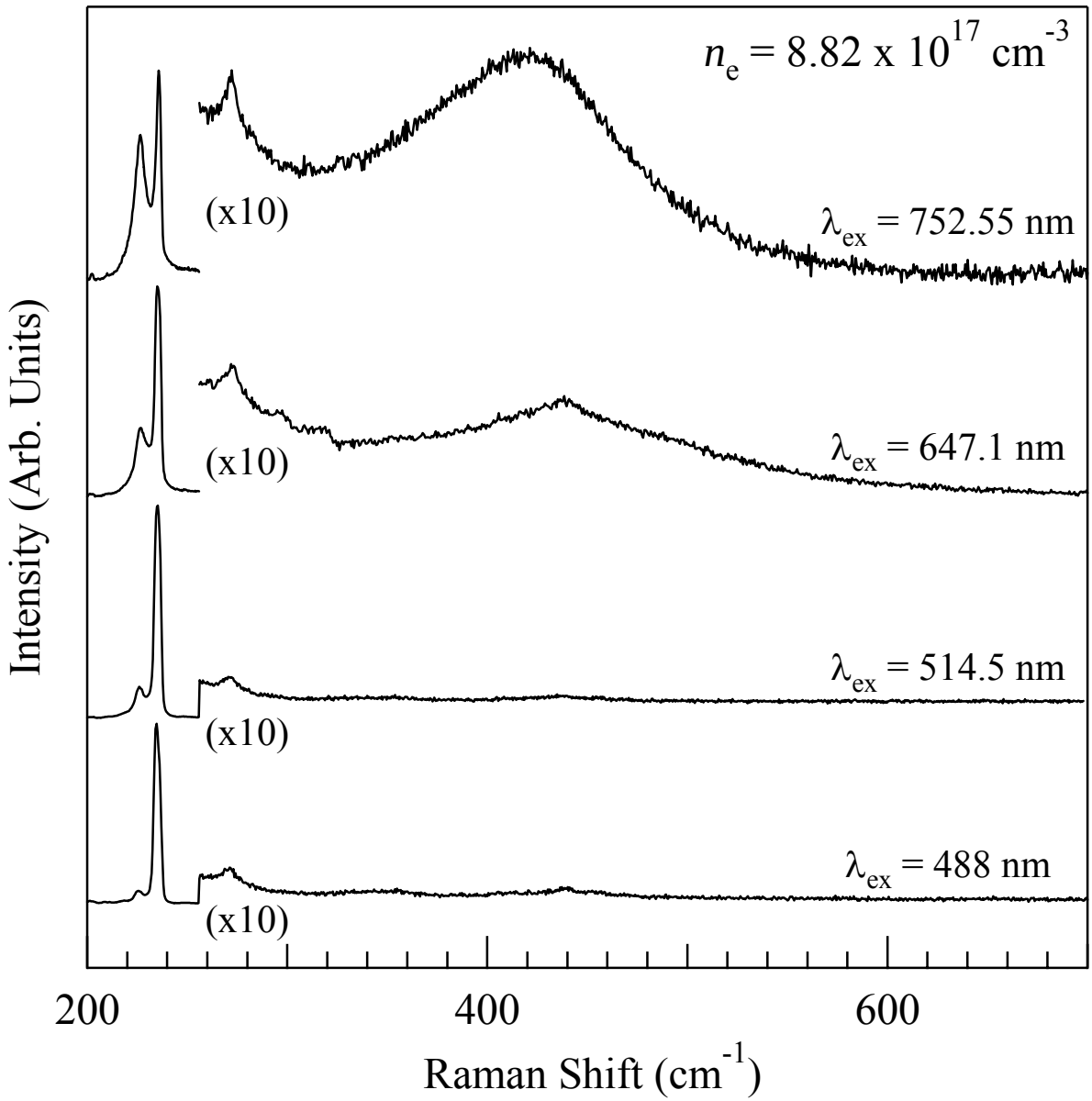
n_e = 8.82 x 10^{17} cm^{-3}
(x10)
λ_{ex} = 752.55 nm
(x10)
λ_{ex} = 647.1 nm
λ_{ex} = 514.5 nm
(x10)
λ_{ex} = 488 nm
(x10)
Intensity (Arb. Units)
200
400
600
Raman Shift (cm^{-1})

Figure 4

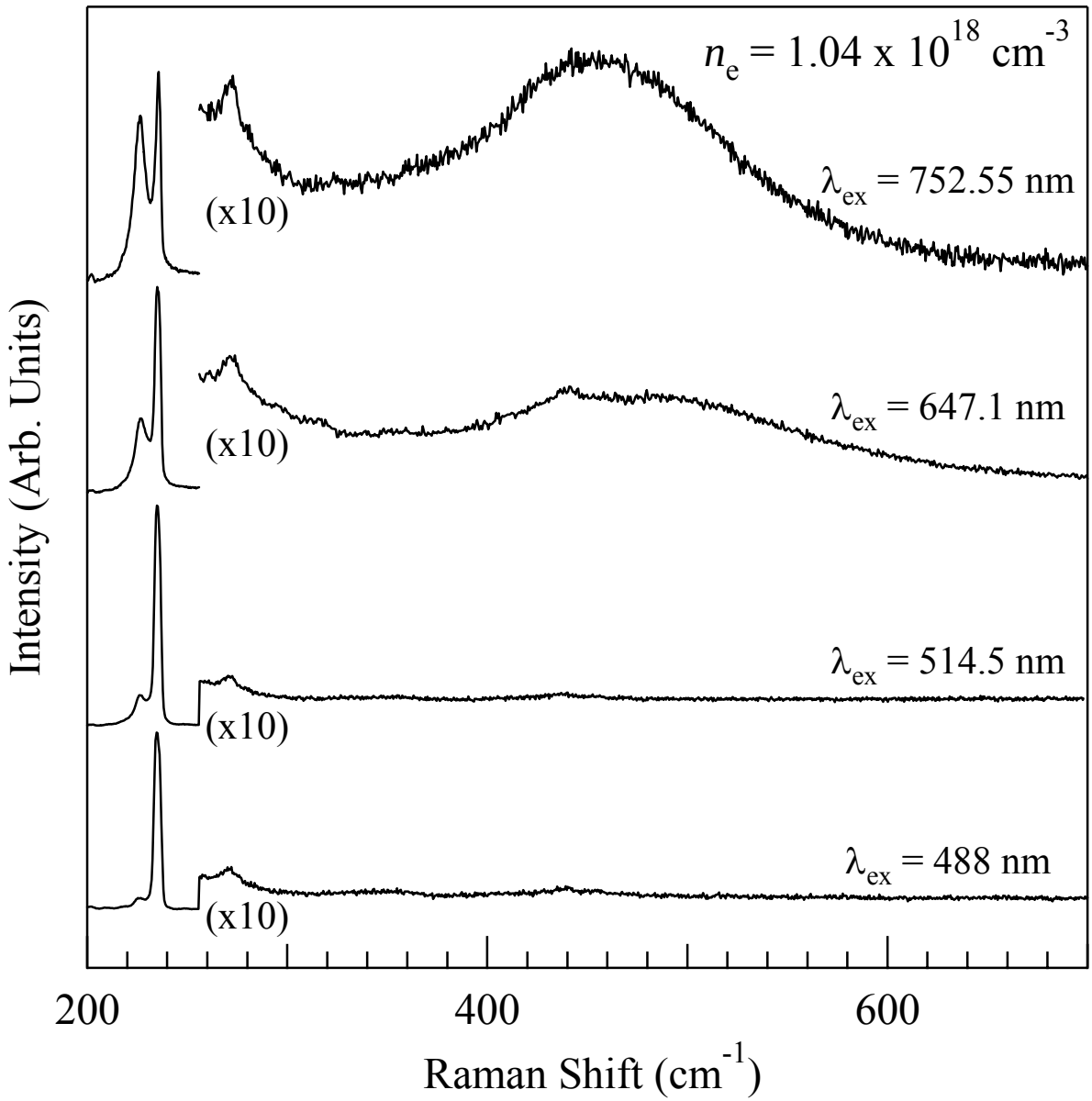
n_e = 1.04 x 10^{18} cm^{-3}
λ_{ex} = 752.55 nm
(x10)
λ_{ex} = 647.1 nm
(x10)
λ_{ex} = 514.5 nm
(x10)
λ_{ex} = 488 nm
(x10)
Intensity (Arb. Units)
200
400
600
Raman Shift (cm^{-1})

Figure 5

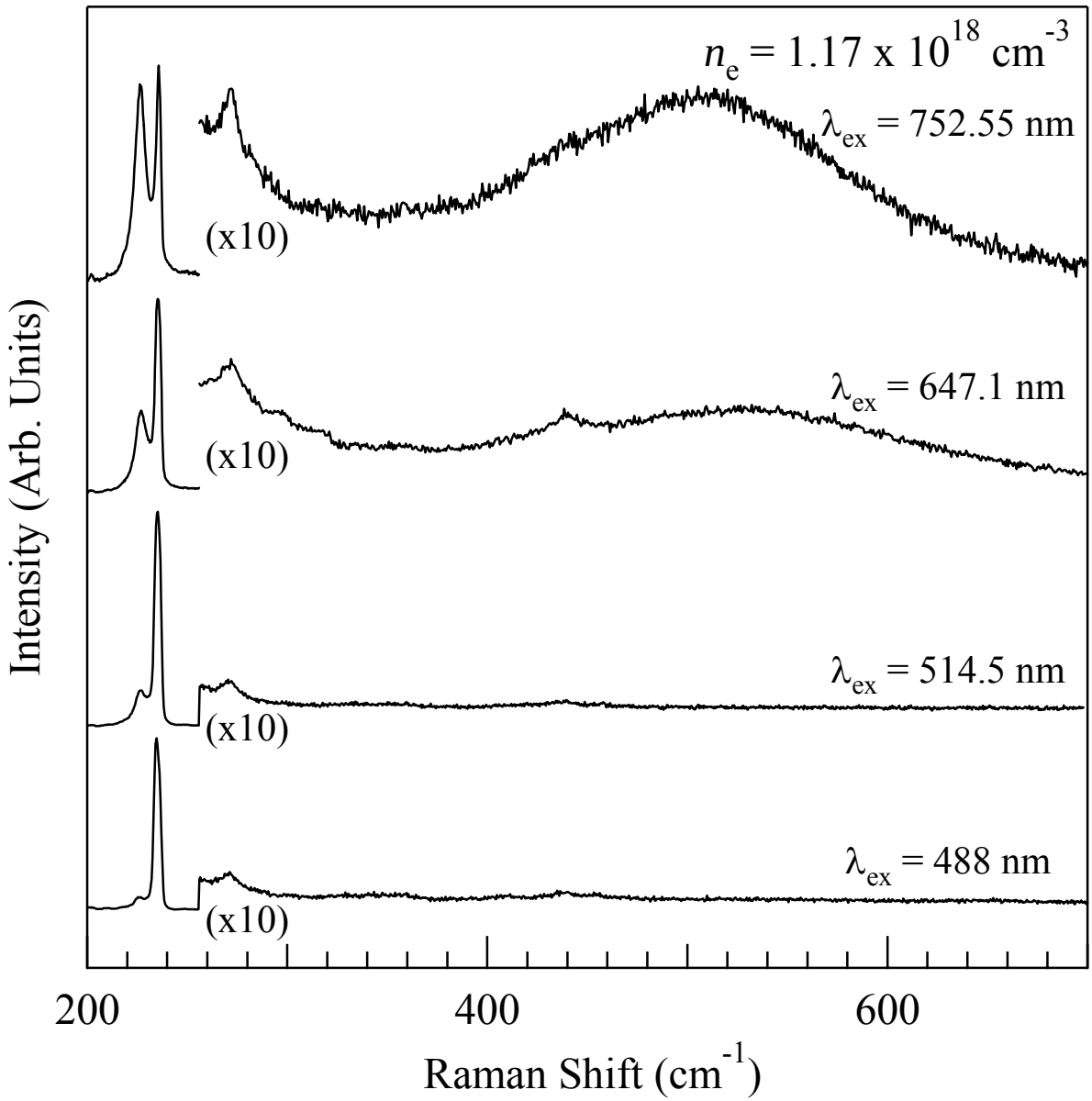
n_e = 1.17 x 10^{18} cm^{-3}
λ_{ex} = 752.55 nm
(x10)
λ_{ex} = 647.1 nm
(x10)
λ_{ex} = 514.5 nm
(x10)
λ_{ex} = 488 nm
(x10)
Intensity (Arb. Units)
200
400
600
Raman Shift (cm^{-1})

Figure 6

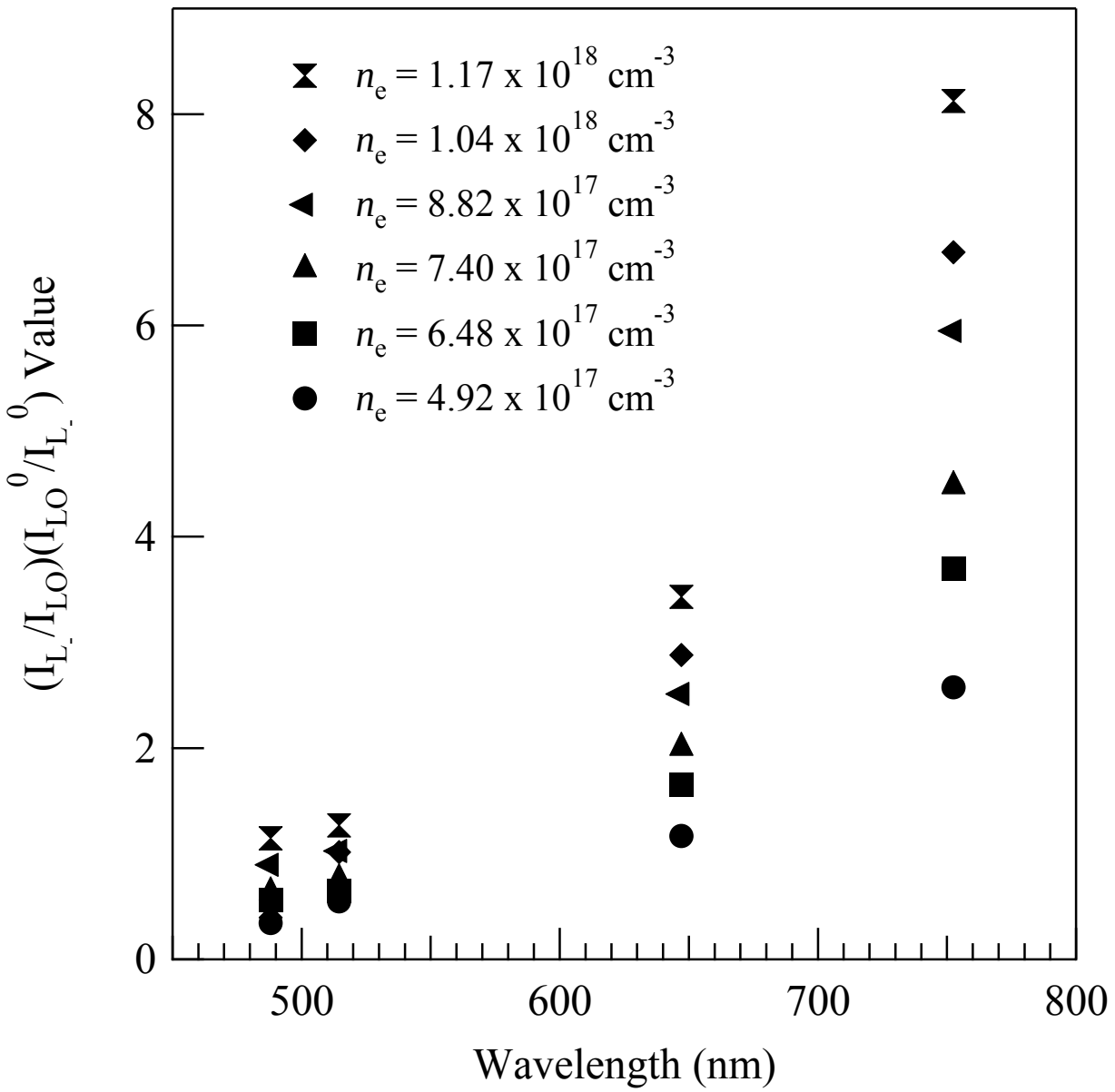
n_e = 1.17 x 10^{18} cm^{-3}
n_e = 1.04 x 10^{18} cm^{-3}
n_e = 8.82 x 10^{17} cm^{-3}
n_e = 7.40 x 10^{17} cm^{-3}
n_e = 6.48 x 10^{17} cm^{-3}
n_e = 4.92 x 10^{17} cm^{-3}
$(I_{L_-}/I_{LO})(I_{LO}^0/I_{L_-}^0)$ Value
0
2
4
6
8
500
600
700
800
Wavelength (nm)

Figure 7

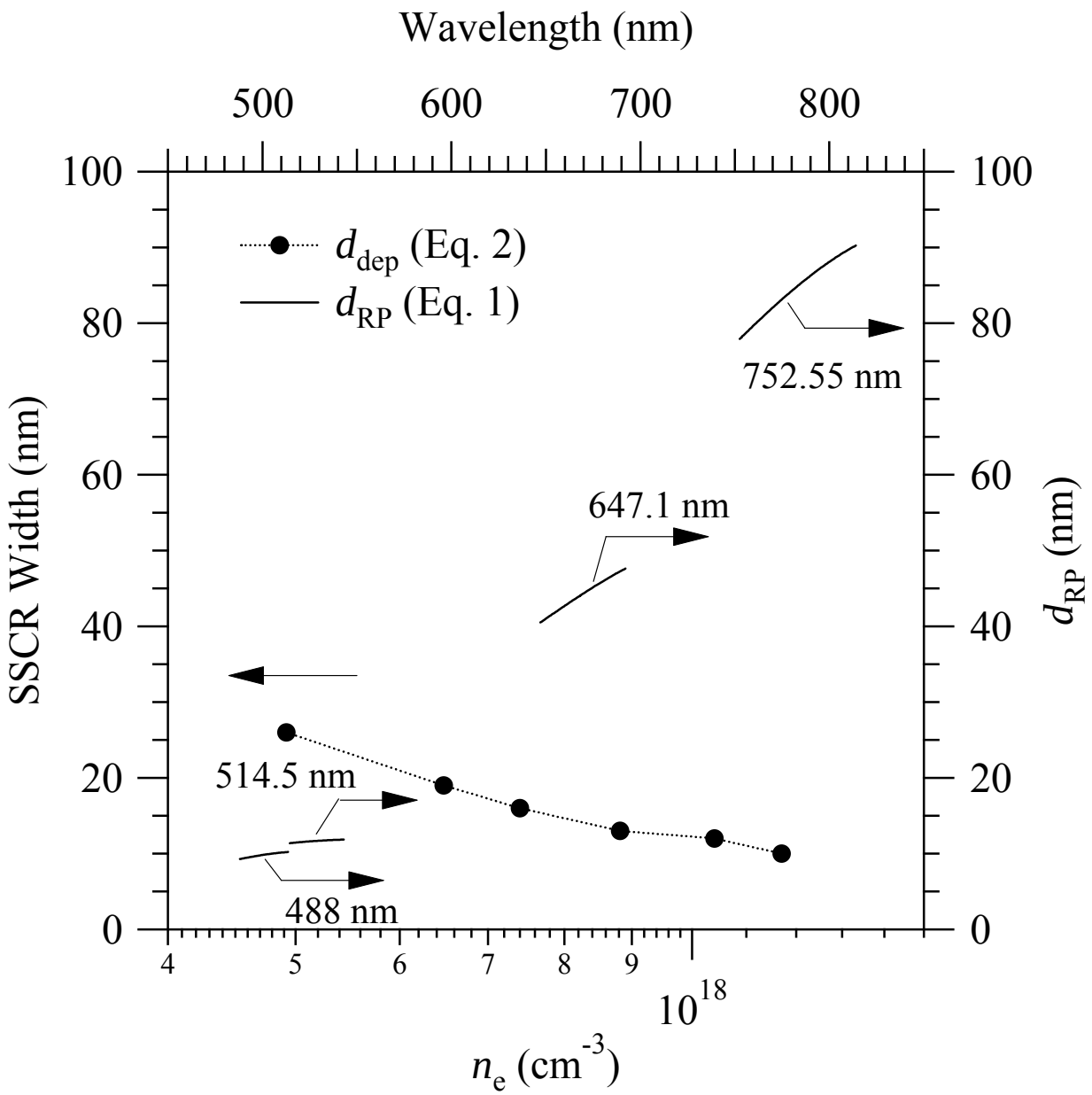
Wavelength (nm)
500
600
700
800
100
80
60
40
20
0
SSCR Width (nm)
d_{dep} (Eq. 2)
d_{RP} (Eq. 1)
752.55 nm
647.1 nm
514.5 nm
488 nm
d_{RP} (nm)
4
5
6
7
8
9
10^{18}
n_e (cm^{-3})

Figure 8

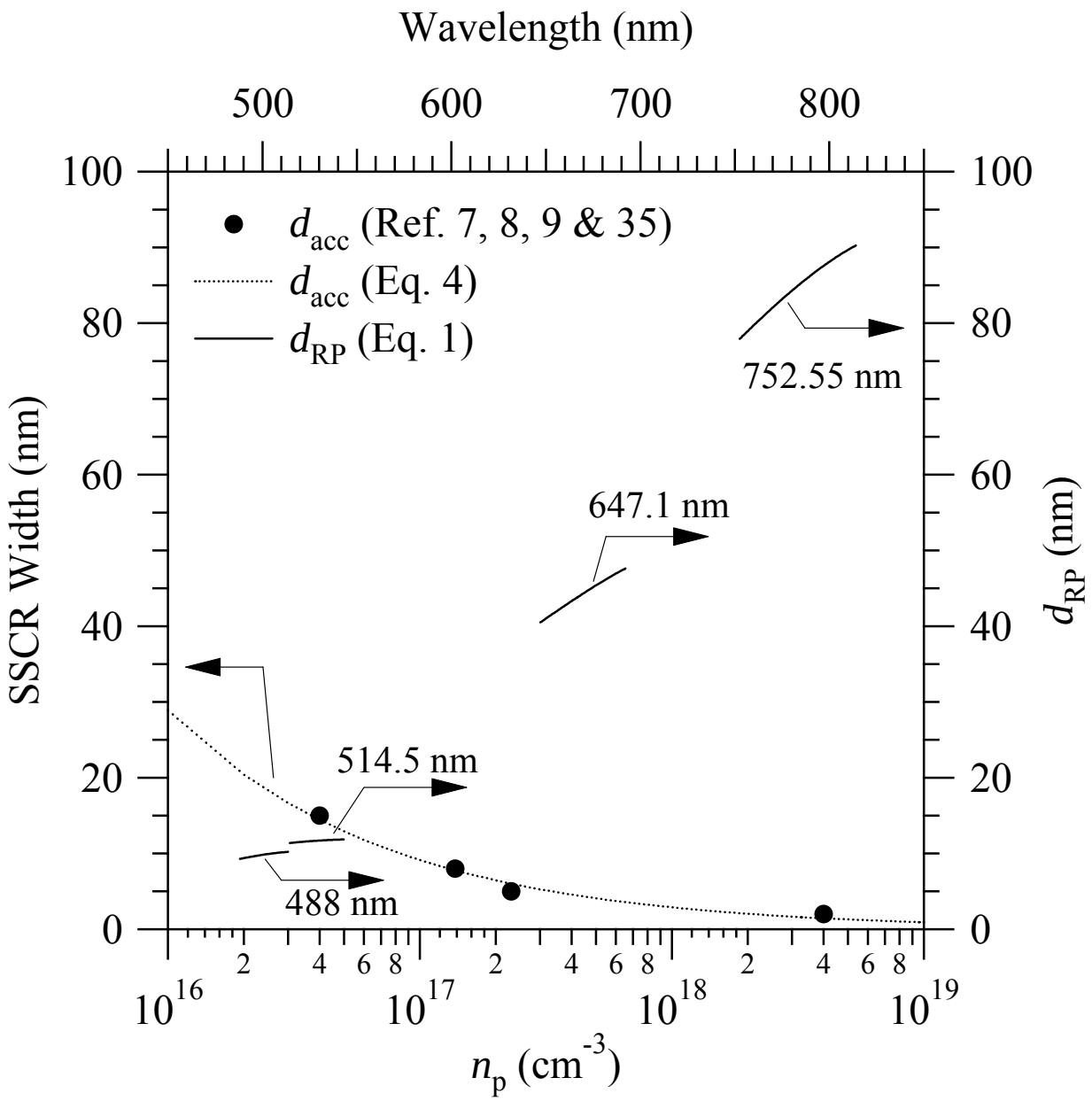
Wavelength (nm)
500
600
700
800
100
80
60
40
20
0
SSCR Width (nm)
d_{acc} (Ref. 7, 8, 9 & 35)
d_{acc} (Eq. 4)
d_{RP} (Eq. 1)
752.55 nm
647.1 nm
514.5 nm
488 nm
d_{RP} (nm)
10^{16}
10^{17}
10^{18}
10^{19}
n_p (cm^{-3})

Figure 9

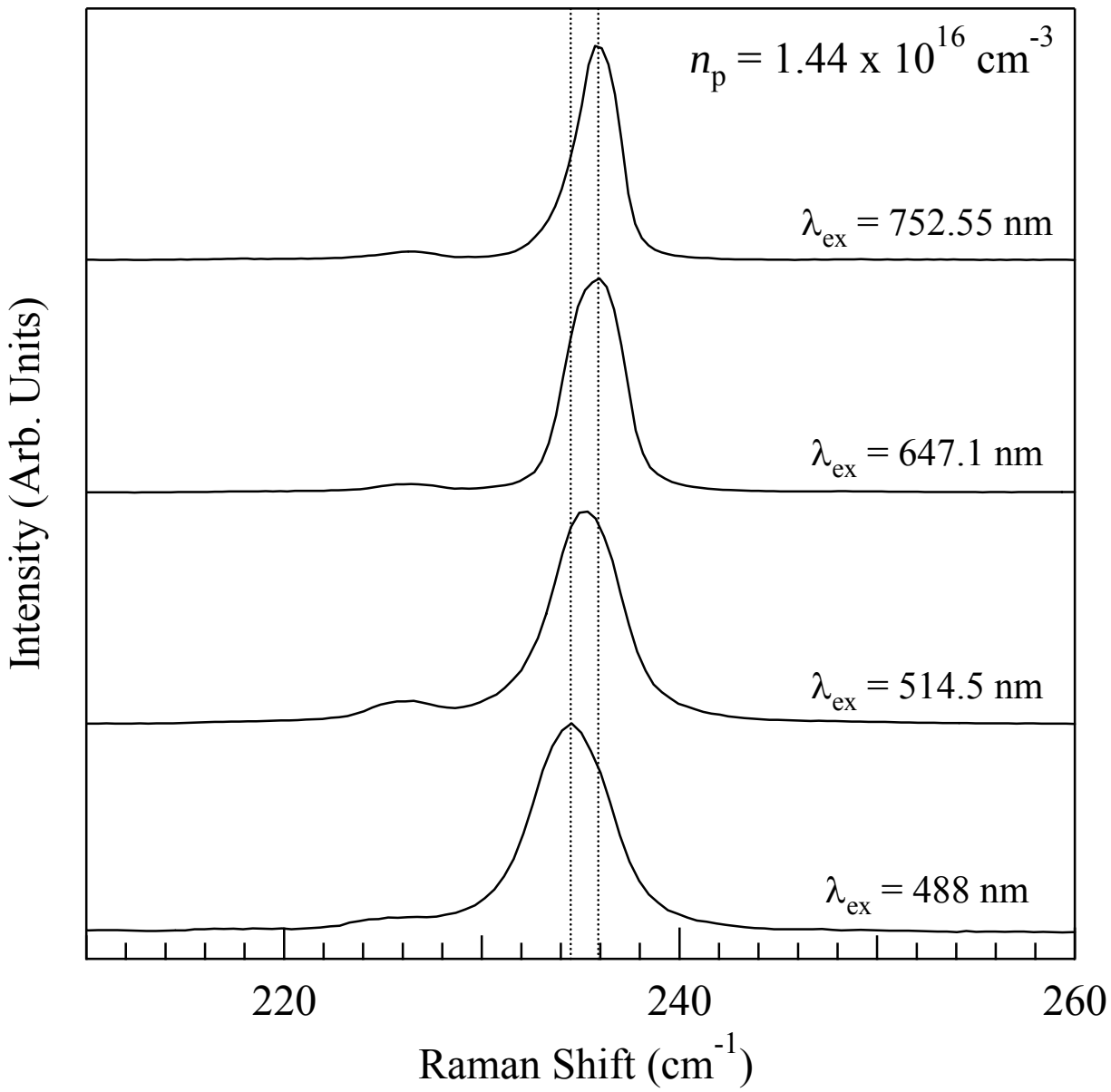
n_p = 1.44 x 10^{16} cm^{-3}
λ_{ex} = 752.55 nm
λ_{ex} = 647.1 nm
λ_{ex} = 514.5 nm
λ_{ex} = 488 nm
Intensity (Arb. Units)
220
240
260
Raman Shift (cm^{-1})

Figure 10

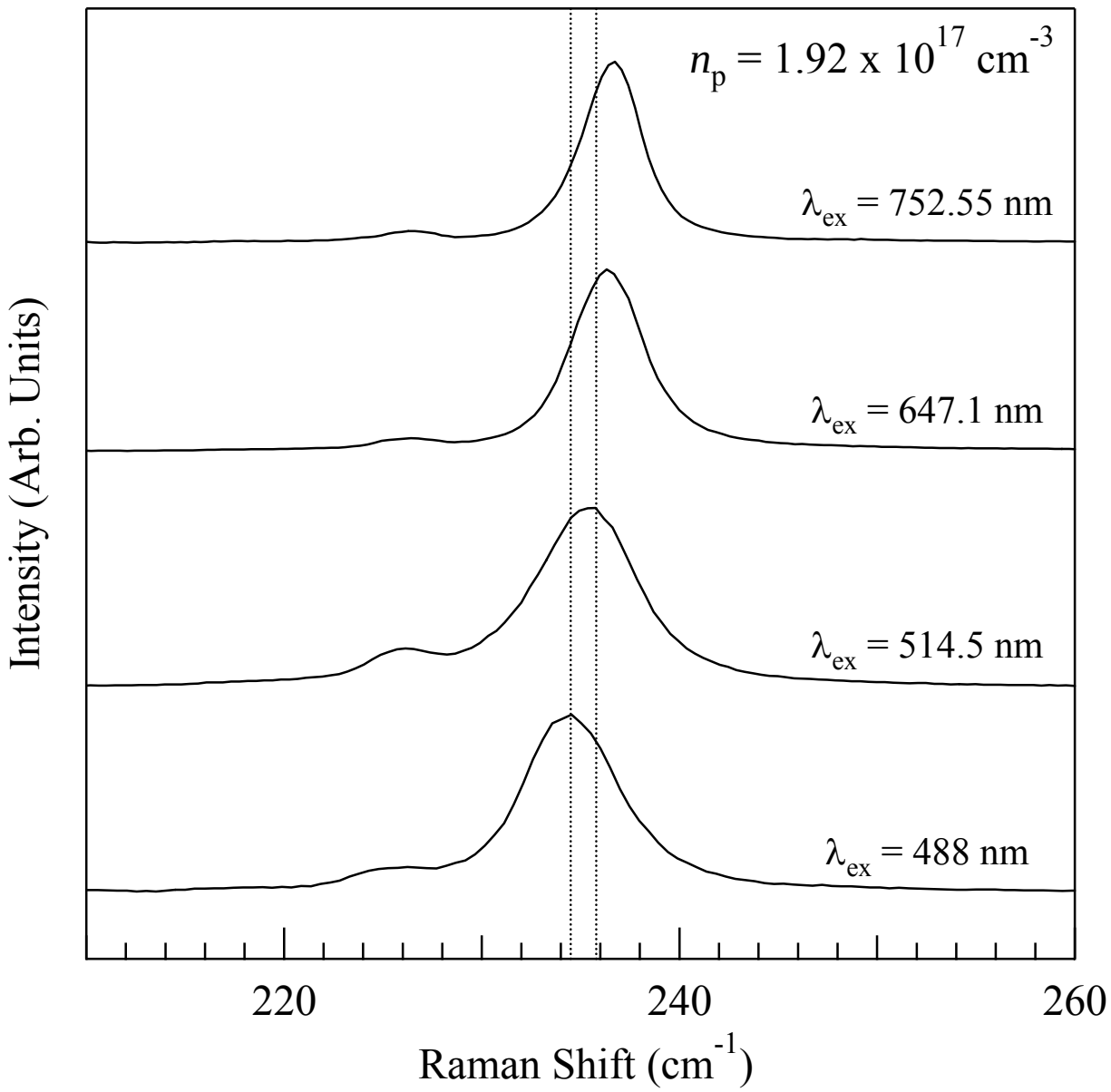
n_p = 1.92 x 10^{17} cm^{-3}
λ_{ex} = 752.55 nm
λ_{ex} = 647.1 nm
λ_{ex} = 514.5 nm
λ_{ex} = 488 nm
Intensity (Arb. Units)
220
240
260
Raman Shift (cm^{-1})

Figure 11

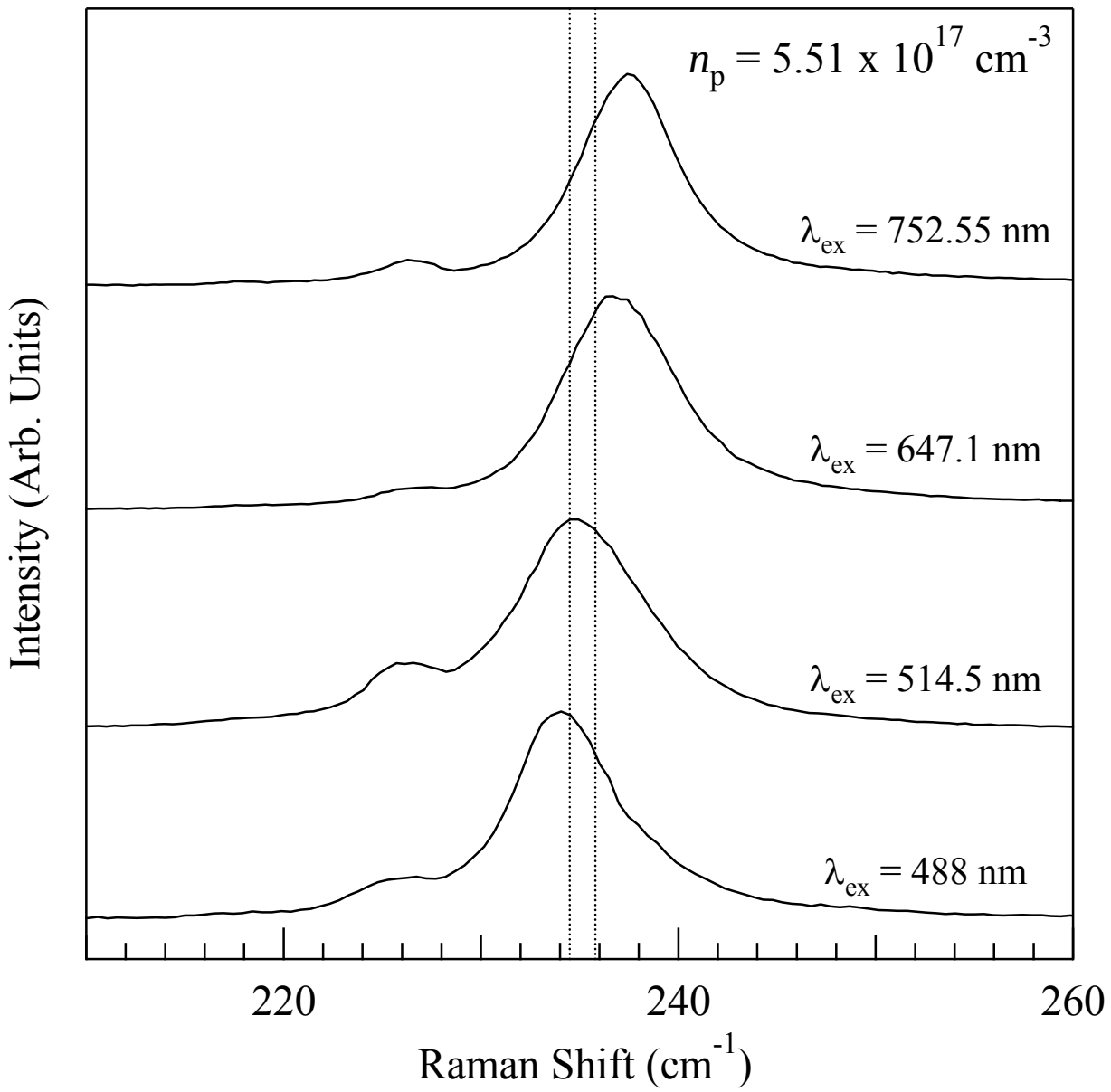
n_p = 5.51 x 10^{17} cm^{-3}
λ_{ex} = 752.55 nm
λ_{ex} = 647.1 nm
λ_{ex} = 514.5 nm
λ_{ex} = 488 nm
Intensity (Arb. Units)
220
240
260
Raman Shift (cm^{-1})

Figure 12

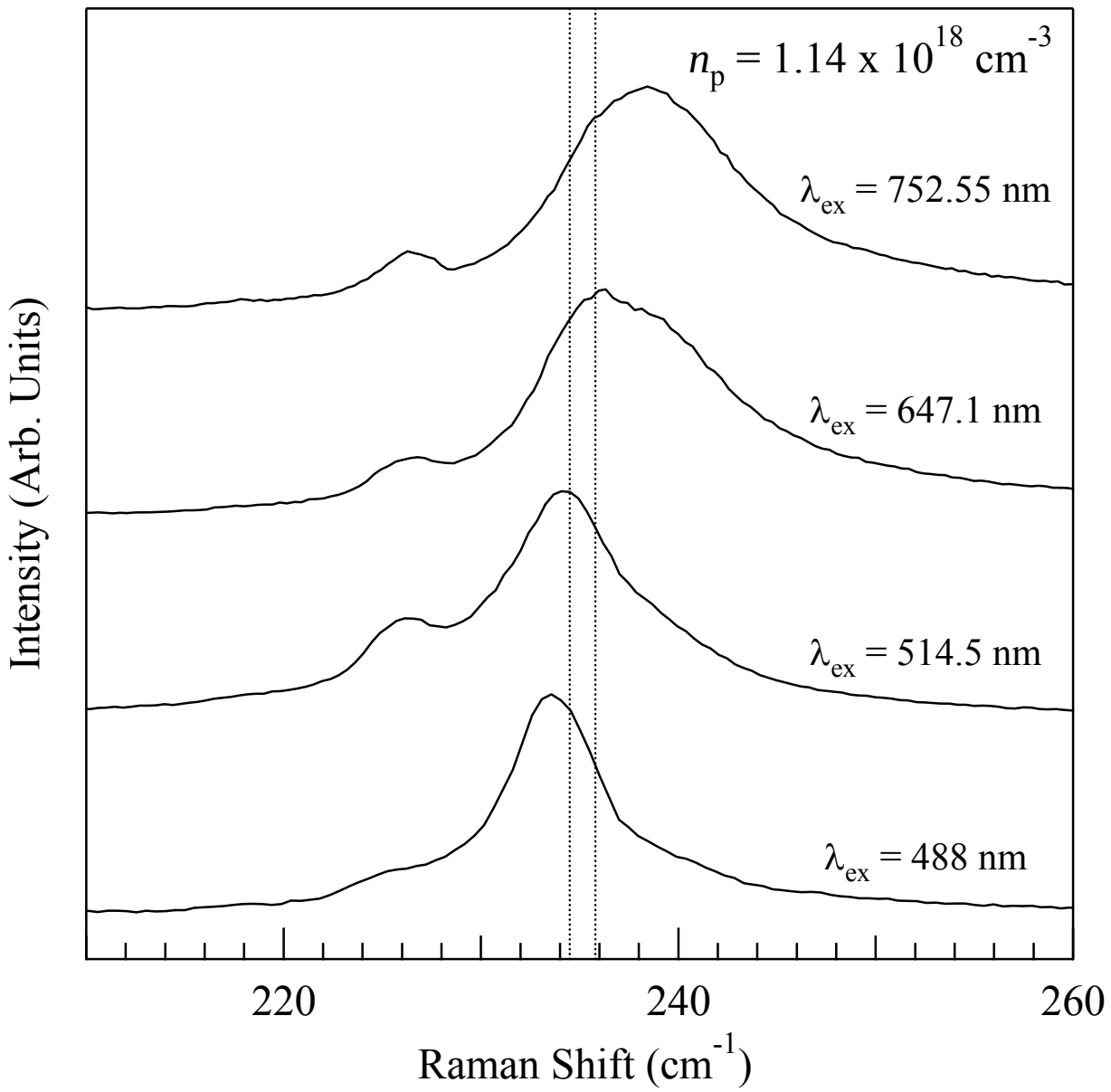
n_p = 1.14 x 10^{18} cm^{-3}
λ_{ex} = 752.55 nm
λ_{ex} = 647.1 nm
λ_{ex} = 514.5 nm
λ_{ex} = 488 nm
Intensity (Arb. Units)
220
240
260
Raman Shift (cm^{-1})

Figure 13

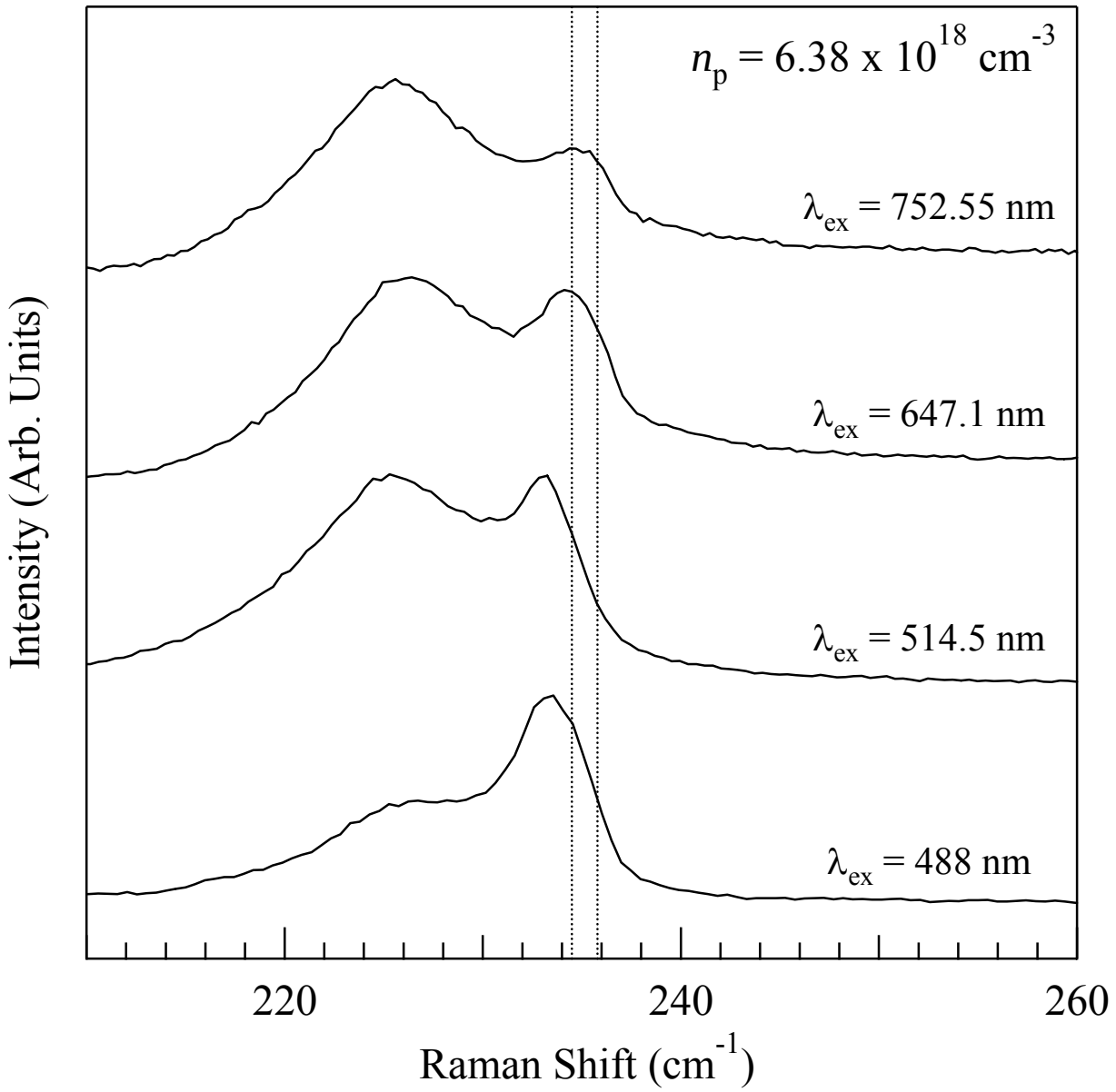
n_p = 6.38 x 10^{18} cm^{-3}
λ_{ex} = 752.55 nm
λ_{ex} = 647.1 nm
λ_{ex} = 514.5 nm
λ_{ex} = 488 nm
Intensity (Arb. Units)
220
240
260
Raman Shift (cm^{-1})

Figure 14